Atmos. Meas. Tech., 9, 6081–6100, 2016
www.atmos-meas-tech.net/9/6081/2016/
doi:10.5194/amt-9-6081-2016

Atmospheric Measurement Techniques
Open Access
EGU

Global distributions of CO_2 volume mixing ratio in the middle and upper atmosphere from daytime MIPAS high-resolution spectra

Á. Aythami Jurado-Navarro[1], Manuel López-Puertas[1], Bernd Funke[1], Maya García-Comas[1], Angela Gardini[1], Francisco González-Galindo[1], Gabriele P. Stiller[2], Thomas von Clarmann[2], Udo Grabowski[2], and Andrea Linden[2]

[1]Instituto de Astrofísica de Andalucía, CSIC, Granada, Spain
[2]Institute for Meteorology and Climate Research (IMK-ASF), Karlsruhe Institute of Technology (KIT), Karlsruhe, Germany

Correspondence to: Manuel López-Puertas (puertas@iaa.es)

Received: 1 March 2016 – Published in Atmos. Meas. Tech. Discuss.: 15 March 2016
Revised: 30 November 2016 – Accepted: 4 December 2016 – Published: 20 December 2016

Abstract. Global distributions of the CO_2 vmr (volume mixing ratio) in the mesosphere and lower thermosphere (from 70 up to ∼ 140 km) have been derived from high-resolution limb emission daytime MIPAS (Michelson Interferometer for Passive Atmospheric Sounding) spectra in the 4.3 µm region. This is the first time that the CO_2 vmr has been retrieved in the 120–140 km range. The data set spans from January 2005 to March 2012. The retrieval of CO_2 has been performed jointly with the elevation pointing of the line of sight (LOS) by using a non-local thermodynamic equilibrium (non-LTE) retrieval scheme. The non-LTE model incorporates the new vibrational–vibrational and vibrational–translational collisional rates recently derived from the MIPAS spectra by Jurado-Navarro et al. (2015). It also takes advantage of simultaneous MIPAS measurements of other atmospheric parameters (retrieved in previous steps), such as the kinetic temperature (derived up to ∼ 100 km from the CO_2 15 µm region of MIPAS spectra and from 100 up to 170 km from the NO 5.3 µm emission of the same MIPAS spectra) and the O_3 measurements (up to ∼ 100 km). The latter is very important for calculations of the non-LTE populations because it strongly constrains the $O(^3P)$ and $O(^1D)$ concentrations below ∼ 100 km. The estimated precision of the retrieved CO_2 vmr profiles varies with altitude ranging from ∼ 1 % below 90 km to 5 % around 120 km and larger than 10 % above 130 km. There are some latitudinal and seasonal variations of the precision, which are mainly driven by the solar illumination conditions. The retrieved CO_2 profiles have a vertical resolution of about 5–7 km below 120 km and between 10 and 20 km at 120–140 km. We have shown that the inclusion of the LOS as joint fit parameter improves the retrieval of CO_2, allowing for a clear discrimination between the information on CO_2 concentration and the LOS and also leading to significantly smaller systematic errors. The retrieved CO_2 has an improved accuracy because of the new rate coefficients recently derived from MIPAS and the simultaneous MIPAS measurements of other key atmospheric parameters (retrieved in previous steps) needed for non-LTE modelling like kinetic temperature and O_3 concentration. The major systematic error source is the uncertainty of the pressure/temperature profiles, inducing errors at midlatitude conditions of up to 15 % above 100 km (20 % for polar summer) and of ∼ 5 % around 80 km. The errors due to uncertainties in the $O(^1D)$ and $O(^3P)$ profiles are within 3–4 % in the 100–120 km region, and those due to uncertainties in the gain calibration and in the near-infrared solar flux are within ∼ 2 % at all altitudes. The retrieved CO_2 shows the major features expected and predicted by general circulation models. In particular, its abrupt decline above 80–90 km and the seasonal change of the latitudinal distribution, with higher CO_2 abundances in polar summer from 70 up to ∼ 95 km and lower CO_2 vmr in the polar winter. Above ∼ 95 km, CO_2 is more abundant in the polar winter than at the midlatitudes and polar summer regions, caused by the reversal of the mean circulation in that altitude region. Also, the solstice seasonal distribution, with a significant pole-to-pole CO_2 gradient, lasts about 2.5 months in each hemisphere, while the seasonal transition occurs quickly.

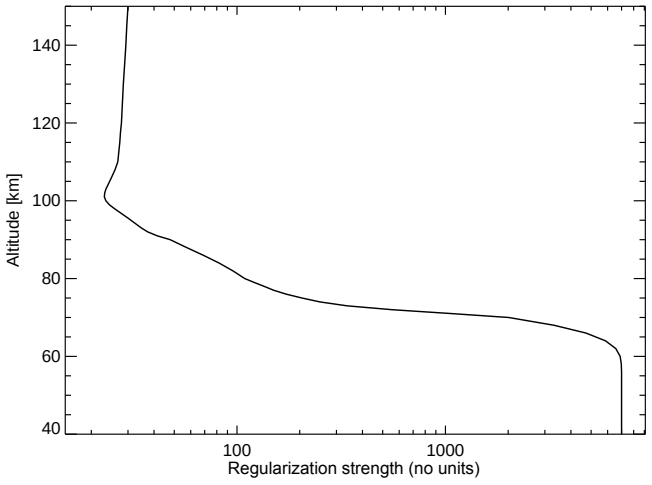

Figure 1. Regularization strength used in the retrieval of the CO_2 vmr.

1 Introduction

Carbon dioxide, CO_2, plays a major role in the radiative energy budget of the atmosphere. Its 15 µm band is the major infrared cooling below around 120 km, and it also causes a significant heating of the upper mesosphere by the absorption of solar radiation in its near-infrared bands (see e.g. López-Puertas and Taylor, 2001). Hence, CO_2 has a critical effect on the atmospheric temperature structure and therefore it is very important to know its global (altitude and latitude) distribution accurately (see e.g. Garcia et al., 2014).

CO_2 was first measured in the upper atmosphere by in situ measurements carried out by rocket-borne mass spectrometers (Offermann and Grossmann, 1973; Trinks et al., 1978; Trinks and Fricke, 1978). The Spectral Infrared Rocket Experiment (SPIRE) measured its 15 µm non-LTE (non-local thermodynamic equilibrium) emission (Stair et al., 1985). The Improved Stratospheric and Mesospheric Sounder (ISAMS) aboard the Upper Atmosphere Research Satellite (UARS) carried out 4.6 µm global measurements performing simultaneous measurements of temperature and pressure up to 80 km (López-Puertas et al., 1998; Zaragoza et al., 2000). CO_2 number densities were retrieved from daytime limb radiance measured by the Cryogenic Infrared Spectrometers and Telescopes for the Atmosphere (CRISTA) measurements in the 60–130 km region (Kaufmann et al., 2002). For a complete review of early measurements until 2000 see López-Puertas et al. (2000). More recently, two satellite CO_2 data sets have been made available. The Fourier transform spectrometer on the Canadian Atmospheric Chemistry Experiment (ACE-FTS) has measured the CO_2 vmr in the mesosphere and lower thermosphere (70 to 120 km) by using the solar occultation technique. This approach has the advantage of being free from non-LTE effects (and the errors associated to the knowledge of the non-LTE population of the emitting states) but provides limited latitudinal coverage (Beagley et al., 2010). Almost simultaneously with ACE, the Sounding of the Atmosphere using Broadband Emission Radiometry (SABER), on board the NASA Thermosphere Ionosphere Energetics and Dynamics (TIMED), has been measuring the atmospheric limb radiance in the 15 and 4.3 µm channels. Rezac et al. (2015) applied a simultaneous temperature–CO_2 vmr retrieval to these measurements and produced a long (13-year) database of CO_2 in the middle and upper atmosphere.

In this paper we describe the inversion of CO_2 vmr from MIPAS (Michelson Interferometer for Passive Atmospheric Sounding) high-resolution daytime limb emission spectra in the 4.3 µm region. MIPAS is able to discriminate the contributions of the many CO_2 bands that give rise to the 4.3 µm atmospheric emission; thus in a previous work it allowed us to obtain a more accurate knowledge of the CO_2 non-LTE processes that control the population of the emitting levels near 4.3 µm (Jurado-Navarro et al., 2015). In that work the large impact of the new collisional rates on the limb atmospheric radiance near 4.3 µm was demonstrated (see Figs. 11 and 12 in that paper). Several tests performed in that study have also shown a substantial effect on the retrieved CO_2. Therefore, the use of those retrieved collisional rates allowed us to retrieve CO_2 with a much better accuracy in the present work than in previous limb emission measurements. In addition, the high spectral resolution allows for a proper selection of the spectral points (optically thin and moderate points of the lines of the bands) containing the largest amount of information at different tangent heights, which constrains the retrieval better than an integral wideband radiance measurement.

In Sect. 2 we describe the MIPAS instrument and the measurements, and in Sect. 3 the retrieval method and the set-up. The advantages of using the CO_2-LOS (line of sight) joint retrieval are discussed in Sect. 4. In Sect. 5 we discuss the major characteristics of the retrieved CO_2 vmr and the error analysis. Finally, in Sect. 6 we provide and discuss a monthly climatology based on the data retrieved in 2010 and 2011. A validation and comparison of MIPAS CO_2 data with ACE and SABER measurements, as well as with Whole Atmosphere Community Climate Model (WACCM) simulations, are to be presented in a future paper.

2 MIPAS observations

The MIPAS instrument is a mid-infrared limb emission spectrometer designed and operated for measurements of atmospheric trace species from space (Fischer et al., 2008). It was part of the payload of Envisat launched on 1 March 2002 with a sun-synchronous polar orbit of 98.55° N inclination and an altitude of 800 km. MIPAS had a global coverage from pole to pole passing the equator from north to south at 10:00 local time, 14.3 times a day and taking daytime and night-time

profiles of spectra. The instrument's field-of-view is 30 km in the horizontal and approximately 3 km in the vertical direction. From January 2005 until the end of Envisat's operations on 8 April 2012, MIPAS measured at a optimized spectral resolution of $0.0625\,\mathrm{cm}^{-1}$.

The MIPAS instrument sounded the middle and upper atmospheres in three measurements modes: MA (middle atmosphere), UA (upper atmosphere) and NLC (noctilucent clouds). The UA mode, scanning the limb from 42 to 172 km, was specifically devised for measuring the thermospheric temperature and CO_2 and NO abundances. In the MA and NLC modes, MIPAS took spectra up to 102 km only. However, since many lines of the CO_2 fundamental band (those with a larger signal) are still optically thick at this tangent height and above, they reduce the sensitivity to the retrieved CO_2 below 102 km. Thus, having measurements above that altitude are very important for retrieving the CO_2 in the optically thin regime and hence better constraining the CO_2 vmr below. As a consequence, the retrieval set-up and the derived CO_2 presented here, data version v5r_CO2_622, correspond to the UA observation mode. Only daytime data were used since the night-time observations are very noisy and non-LTE processes are not known that accurately. Note that the three MIPAS modes have very similar temporal and latitudinal coverages. Hence the retrieval of CO_2 from the MA and NLC modes would not significantly extend the coverage of the CO_2 UA database. The limb vertical sampling of the UA mode is 5 km from 172 km down to 102 km and 3 km below, recording a rear viewing sequence of 35 spectra every 63 s. Its along-track horizontal sampling is of about 515 km (De Laurentis, 2005; Oelhaf, 2008). Version V5 (5.02/5.06) of the L1b calibrated and geo-located spectra processed by the European Space Agency (ESA; Perron et al., 2010; Raspollini et al., 2010) were used here for the retrieval of CO_2 and for all other parameters used in its retrieval, namely, pressure/temperature and ozone.

3 The retrieval method and its set-up

Carbon dioxide vmr profiles together with the elevation pointing of the line of sight (LOS) are retrieved using the MIPAS level 2 processor developed and operated by the Institute of Meteorology and Climate Research (IMK) together with the Instituto de Astrofísica de Andalucía (IAA). The processor is based on a constrained non-linear least squares algorithm with Levenberg–Marquardt damping (von Clarmann et al., 2003). Its extension to retrievals with consideration of non-LTE (i.e. CO, NO and NO_2) is described by Funke et al. (2001). Non-LTE vibrational populations of CO_2 are modelled with the Generic RAdiative traNsfer AnD non-LTE population Algorithm (GRANADA; Funke et al., 2012; see more details below) within each iteration of the retrieval.

Following the scheme described by von Clarmann et al. (2003), the following retrieval equation is used:

$$\boldsymbol{x}_{i+1} = \boldsymbol{x}_i + \left[\mathbf{K}^T \mathbf{S}_y^{-1} \mathbf{K} + \mathbf{R} + \lambda \mathbf{I}\right]^{-1} \times \left\{\mathbf{K}^{\mathbf{T}} \mathbf{S}_y^{-1} [\boldsymbol{y}_{\mathrm{meas}} - \boldsymbol{y}(\boldsymbol{x}_i)] - \mathbf{R}(\boldsymbol{x}_i - \boldsymbol{x}_a)\right\}, \quad (1)$$

where $\mathbf{K}$ is the $m_{\max} \times n_{\max}$ Jacobian, containing the partial derivatives of all $m_{\max}$ simulated measurements $\boldsymbol{y}(\boldsymbol{x})$ under consideration with respect to all unknown parameters $\boldsymbol{x}$, superscript $\mathbf{T}$ denotes a transposed matrix, $\boldsymbol{x}$ is the $n_{\max}-$dimensional vector of unknown parameters and $\boldsymbol{x}_a$ is the related a priori information. The term $\boldsymbol{y}_{\mathrm{meas}}$ is the $m_{\max}$-dimensional vector of measurements under consideration, $\boldsymbol{y}(\mathbf{x_i})$ is the forward modelled spectrum using parameters $\mathbf{x_i}$ from the i-th step of iteration. $\mathbf{R}$ is an $n_{\max} \times n_{\max}$ regularization matrix, and $\mathbf{S}_y$ is the $m_{\max} \times m_{\max}$ covariance matrix of the measurement. The term $\lambda\mathbf{I}$ (tuning scalar times the unity matrix) dampens the step width $\boldsymbol{x}_{i+1} - \boldsymbol{x}_i$, bends its direction toward the direction of the steepest descent of the cost function in the parameter space and prevents a single iteration from causing a jump of parameters $\boldsymbol{x}$ beyond the linear domain around the current guess $\boldsymbol{x}_i$ (Levenberg, 1944; Marquardt, 1963).

In our case, the column vector $\boldsymbol{x}$ contains the CO_2 profile (103 elements), the LOS profile (23 elements) and the radiance offset (17 elements, one per each microwindow). The a priori profile, $\boldsymbol{x}_a$, for CO_2 is taken from monthly zonal means of the Whole Atmosphere Community Climate Model with specified dynamics (SD-WACCM) simulations spanning over the time period of the measurements (Garcia et al., 2014). SD-WACCM is constrained with output from NASA's Modern-Era Retrospective Analysis (MERRA) (Rienecker et al., 2011) below approximately 1 hPa. Garcia et al. (2014) showed SD-WACCM simulations for Prandtl numbers (P_r) of 4 (standard) and 2, corresponding to lower and higher eddy diffusion coefficients respectively. Here we used the simulations for $P_r = 2$, which gives an overall better agreement with ACE CO and CO_2 and MIPAS CO (Garcia et al., 2014). In this way we expect to have a faster convergence with no impact of the a priori profile since the CO_2 profile is regularized by means of a Tikhonov-type first-order smoothing constraint (Tikhonov, 1963; see below). The a priori profile for the elevation pointing of the line of sight (LOS) was taken from that retrieved from the 15 µm region (García-Comas et al., 2014).

Since in the target altitude range we use a smoothing constraint only, $\boldsymbol{x}$ is not pushed towards the a priori profile but the latter constrains the shape of the resulting profile only. $\mathbf{S}_y$ is the covariance matrix characterizing the measurement noise. Due to apodization (Norton and Beer, 1976) this matrix contains off-diagonal elements. $\mathbf{R}$ is the constraint matrix. CO_2 is constrained by a Tikhonov-type (Tikhonov, 1963) squared first-order finite differences matrix (weighted by the grid-width) with altitude-dependent regu-

Table 1. Errors of the CO_2 vmr retrieved in this work for the midlatitude and polar summer (in parenthesis) conditions.

	Errors (%)							
Height (km)	Random	Temperature	O(^1D)	O(^3P)	Gain (1.25 %)	Solar flux (1 %)	Abs. pointing	Total (sys.)
70	< 1 (< 1)	0.33 (0.12)	0.21 (0.26)	0.10 (0.09)	0.08 (0.18)	0.03 (0.12)	0.0	0.41 (0.37)
75	1 (1)	3.3 (0.9)	1.8 (2.4)	0.8 (0.7)	0.7 (1.7)	0.24 (1.2)	0.1	3.9 (3.4)
80	1 (1)	5.1 (0.13)	2.1 (2.7)	0.44 (0.4)	0.8 (2.0)	0.02 (1.1)	0.3	5.6 (3.6)
85	1 (1)	3.2 (1.6)	1.2 (1.3)	0.12 (0.17)	0.67 (1.1)	0.19 (0.18)	0.4	3.5 (2.4)
90	2 (2)	1.5 (0.02)	1.4 (1.4)	0.44 (0.16)	0.8 (1.1)	0.16 (0.12)	0.5	2.3 (2.0)
95	3 (3)	1.0 (5.4)	1.0 (0.6)	0.03 (0.9)	0.45 (0.08)	0.6 (1.2)	0.5	1.7 (5.6)
100	3 (3)	4.4 (19)	1.1 (4)	1.4 (3.4)	0.34 (2.0)	1.4 (2.8)	1.1	5.1 (20)
105	4 (4)	9 (22)	2.5 (4)	1.6 (3.5)	0.6 (1.8)	1.4 (2.2)	1.3	10 (22)
110	5 (4)	11 (21)	3.1 (3.2)	2.5 (3.4)	0.9 (1.3)	1.4 (1.7)	1.5	12 (22)
115	5 (5)	10 (24)	1.1 (1.6)	2.2 (2.7)	0.01 (0.34)	0.7 (0.9)	1.1	11 (24)
120	6 (5)	11 (24)	0.6 (0.6)	0.8 (2.0)	0.8 (0.02)	0.02 (0.6)	0.7	11 (24)
125	7 (7)	12 (22)	1.2 (0.3)	0.13 (1.0)	0.9 (0.31)	0.25 (0.32)	0.7	12 (22)
130	9 (9)	13 (21)	1.5 (1.1)	0.9 (0.06)	1.1 (0.6)	0.4 (0.07)	0.7	13 (21)
135	11 (12)	13 (20)	2.1 (1.7)	2.1 (0.9)	1.5 (0.9)	0.7 (0.13)	0.5	14 (20)
140	13 (14)	14 (20)	2.8 (2.2)	3.4 (1.5)	1.2 (1.1)	1.1 (0.28)	0.1	15 (20)

larization strength (von Clarmann et al., 2003). The regularization strength used here is shown in Fig. 1. Using those values, the constraint is optimized to obtain stable calculations but with a precision high enough to allow for physically meaningful variations of the retrieved CO_2 abundance.

In addition, a strong diagonal constraint is added below 60 km in order to force the retrieved CO_2 to be close to the well-known mixing ratio in the lower mesosphere. The entries correspond to the CO_2 a priori standard deviations of ~ 0.5 %, in line with the errors of the CO_2 vmr in the 5–25 km region retrieved from ACE spectra (Foucher et al., 2011). Admittedly the combination of a smoothing constraint with a diagonal constraint at low altitudes also forces the result towards the a priori profile in a certain altitude range above the threshold altitude where the diagonal constraint is active. This effect, however, dampens out very quickly (see e.g. Fig. 13a and b).

A Tikhonov first-order smoothing constraint is also used for the LOS retrieval, allowing for vertically coarse variations of $\sim$ 10–20 km of the tangent height spacing with respect to the a priori profile. The LOS of the lowermost tangent height is strongly constrained to the a priori profile by means of a diagonal regularization. Typically, the obtained degrees of freedom for the LOS retrievals are about 2.

The Levenberg–Marquardt parameter λ scales unity $\mathbf{I}$. It is zero by default and is set to positive values only when the retrieval is found to diverge. Linearity is checked explicitly along with the convergence test by comparing the modelled and linearly extrapolated spectrum. A retrieval counts as converged only if the linear prediction of the n-1st step is close enough to the explicit non-linear line-by-line calculation of the nth step. The stopping criterion is defined such that convergence is reached for both the residual spectra and the retrieval parameter vector. The typical number of iterations is in the range of 3 to 6 and the convergence percentage is very high, about 99.4 %. For further details like the cost function we refer the reader to von Clarmann et al. (2003).

Besides the CO_2 vmr profile and LOS, a height- and wavenumber-independent radiance offset is also fitted jointly in the retrieval. Before starting the retrieval, the L1b spectra were corrected for the spectral shift. The temperature used in the retrieval was taken from that retrieved from the same MIPAS spectra in the 15 µm region (García-Comas et al., 2014) below around 100 km, and that retrieved from the same MIPAS spectra in the NO 5.3 µm emission (Bermejo-Pantaleón et al., 2011) from 100 up to 170 km. Both temperatures were merged in the 95–105 km region using a hyperbolic tangent function.

Pressure was implicitly determined by means of hydrostatic equilibrium (total density was obtained from pressure and temperature and using the ideal gas law). The CO_2 non-LTE model used in the non-LTE inversion is described in detail in Funke et al. (2012). However, the collisional coefficients of many vibrational–vibrational and vibrational–translational processes were updated with the values retrieved from MIPAS spectra as described in Jurado-Navarro et al. (2015). In addition, some of the collisional rates of that work were updated here because of the improvements in the calculation of the O(^1D) concentration (see below) and further refinements leading to smaller residual spectra. These updates include, first, the collisional rates of $CO_2(v_d, v_3)$ + M $\leftrightharpoons$ $CO_2(v'_d, v_3 - 1)$ + M with $\Delta v_d = 2 - 4$ and M = N_2, O_2 (processes 8a and 8b in Table 1 of Jurado-Navarro et al., 2015) where the factor f has been changed from 0.82 to 0.7. Secondly, the rate of $N_2(1) + O \rightarrow N_2 + O$ (process 10 in that table) has been updated with a rate coefficient of 4.5×10^{-15}

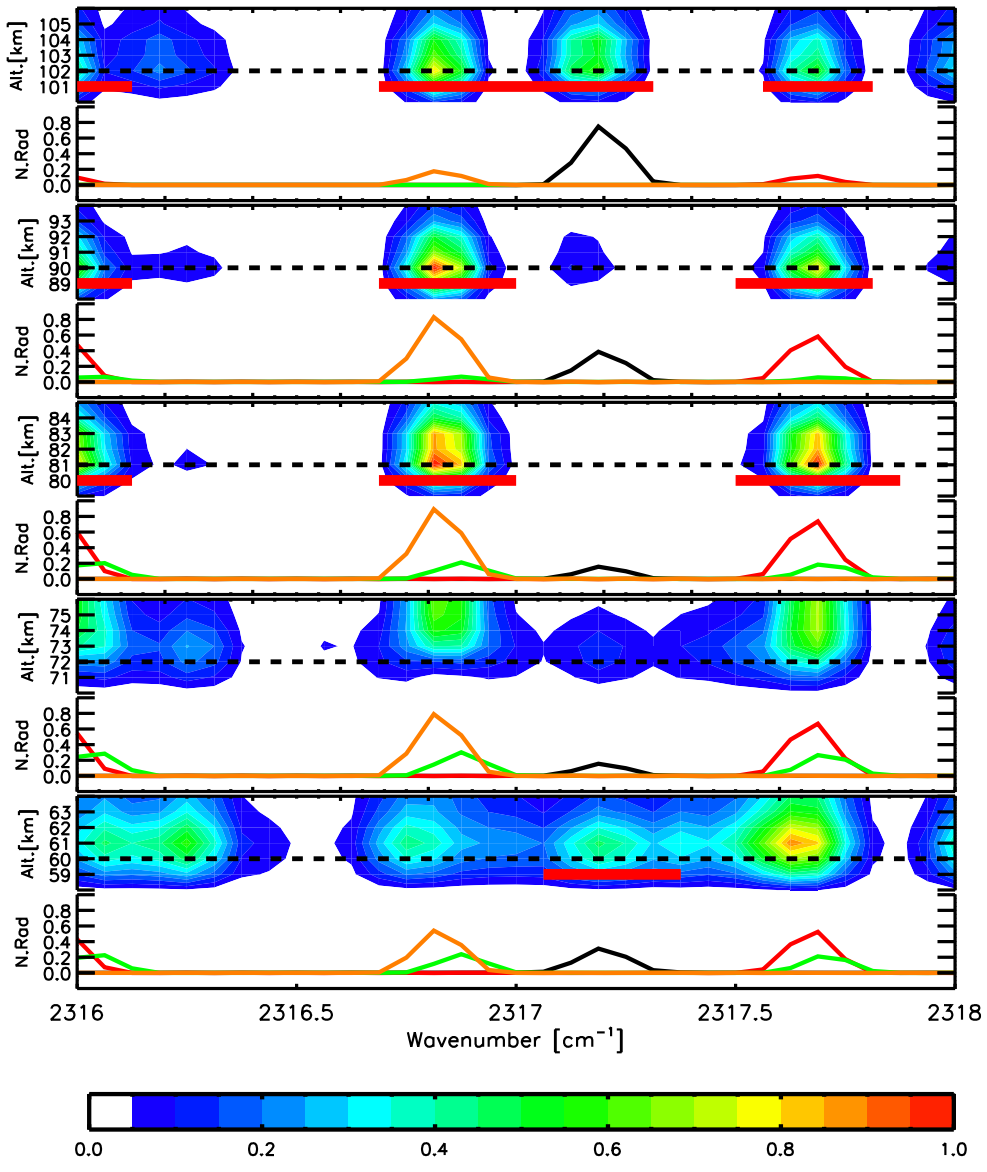

Figure 2. Jacobians in the 2316–2318 cm^{-1} region for five different tangent altitudes (from bottom to top: 60, 72, 81, 90 and 102 km). Two panels are shown for each tangent altitude. Upper panel: normalized Jacobians where the dashed black line indicate the tangent altitude and the thick red line the micro-window extension. As a guide, the lower panels show the normalized radiance contributions for the most prominent CO_2 lines: of the fundamental band (black), of the second hot $10^01 \rightarrow 10^00$ band (red), of the $02^21 \rightarrow 02^20$ band (green) and of $02^01 \rightarrow 02^00$ (orange).

$(T/300)^{1.5}$ cm^3 s^{-1} and $f = 1$. This rate has been adapted from Whitson and McNeal (1977), taking the upper limit (within the error bars) at 300 K, and re-adjusting the temperature dependence, taking into account the measurements at higher temperatures. The values of this new rate at temperatures near 300 K are, however, similar to those used in Jurado-Navarro et al. (2015).

The non-LTE model also requires other input quantities that affect the non-LTE populations of the emitting states. In particular it requires the concentrations of O_3, $O(^3P)$ and $O(^1D)$. For ozone we used that retrieved from the same MIPAS spectra in the 10 µm spectral region (Gil-López et al., 2005; Smith et al., 2013) below 100 km. The atomic oxygen and $O(^1D)$ profiles below 100 km were generated from the O_3 retrieved from the same MIPAS spectra and the photochemical model described by Funke et al. (2012). Above 100 km, we took the atomic oxygen and O_2 concentrations from the NRLMSIS-00 model (Picone et al., 2002). The $O(^1D)$ profile above 100 km has been updated from the photochemical model by Funke et al. (2012), using the O_2 photoabsorption cross sections from Ogawa and Ogawa (1975) and Lu et al. (2010), and a new efficiency of $O(^1D)$ production

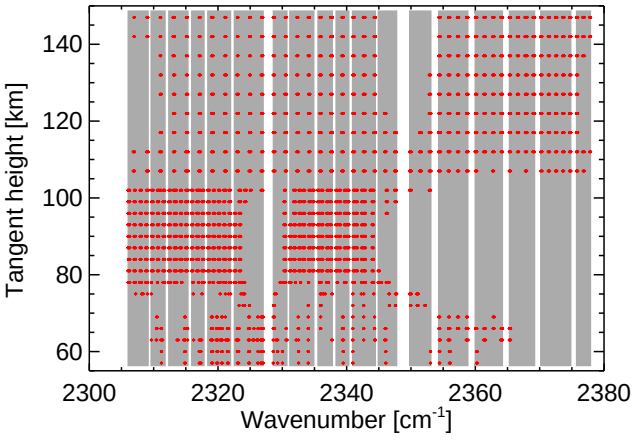

Figure 3. Occupation matrix used in the CO_2 retrieval in the 4.3 µm spectral region. Shaded regions represent the spectral regions selected and red dots the microwindow mask at each tangent height. The specific microwindows used in the retrieval are listed in the Supplement.

from O_2 photo-absorption that considers that, at wavelengths shorter than ~ 100 nm the O_2, ionization is the dominant channel. We also included an overhead column above the top layer of the model proportional to the scale height of O_2. This $O(^1D)$ photo-production has been compared with that calculated for similar conditions by an independent UV radiative transfer model (González-Galindo et al., 2005; Garcia et al., 2014), finding differences smaller than 2 % at all altitudes. A variable solar spectral irradiance (SSI; Lean et al., 2005) was included in all the photochemical calculations in order to account for solar UV variations along the MIPAS observation period.

The retrievals are performed from 42 up to 152 km, over a discrete altitude grid of 1 up to 50, 2 from 50 to 70, 1 from 70 to 80, 2 from 80 to 90, 1 from 90 to 110, 2.5 from 110 to 120 and 5 from 120 to 152 km. The selected grid provides balanced accuracy and efficiency. The forward calculations are performed at that grid but using an internal sub-grid to achieve very accurate radiances. The over-sampled retrieval grid, finer than the MIPAS vertical measurement grid (varying from ≈ 3 below 100 km to ≈ 5 km above that altitude), makes the use of a regularization mandatory in order to obtain stable solutions. In the retrieval we use only the spectra taken in the tangent altitude range from 60 up to 142 km. The spectra above 142 km have a low signal-to-noise ratio and did not contain significant information. The numerical integration of the signal over the vertical field-of-view (≈ 3 km or ≈ 5 km) is done using seven pencil beams. The forward model calculations along the line of sight (LOS) include gradients (along the LOS) in the non-LTE populations of the emitting levels caused by both kinetic temperature gradients as well as by different solar illumination conditions (variable solar zenith angle) along the LOS.

The retrievals are performed using selected spectral regions (micro-windows) in the 4.3 µm region in MIPAS channel D (1820–2410 cm^{-1}), which vary with tangent altitude, in order to optimize computation time and minimize systematic errors (von Clarmann and Echle, 1998). In particular, error propagation due to horizontal inhomogeneities have been minimized by excluding opaque spectral lines which are insensitive to tangent point conditions.

The selection of the spectral regions sensitive to the CO_2 abundance is performed by calculating the 4.3 µm Jacobians and selecting those regions with a good local response. In this way, and thanks to the excellent MIPAS spectral resolution, we are able to select the spectral points sensitive to the CO_2 vmr, yet with a good signal-to-noise ratio, while excluding lines with non-local responses due to spectral saturation. We have selected 18 principal spectral regions within the 2300–2380 cm^{-1} range, containing height-dependent microwindows at 23 tangent heights from 60 up to 142 km. An illustration of the selection for a particular spectral region is shown in Fig. 2. At 60 km, the fundamental band line (black) shows a local response and hence it is selected in the microwindows mask. On the contrary, the second hot lines (red and orange) do not give a local response (the Jacobians are much more extended in altitude or their maxima occur at altitudes well above the tangent height) and hence are not selected. They are, however, included in the microwindow mask for higher tangent heights, i.e. from 85 up to 102 km, where they have quite enough local sensitivity. In this example the fundamental band line is not selected from 72 to 90 km, although it again gives valuable information at 102 km. Around 100 km the information progressively comes from lines in the second hot band to those in the fundamental band.

In addition to the exclusion of spectral points with non-local response, we restricted the microwindows to the strongest lines (mainly fundamental and second hot bands lines that have the larger signal/noise ratio) at each altitude for reasons of computational efficiency. Additionally, spectral regions with interferences from the 636, 628, 627, 638 and 637 CO_2 isotopologues have been suppressed in order to avoid systematic errors caused by the less accurate non-LTE modelling of these minor species, since the collisional rates affecting these energy levels were not retrieved by Jurado-Navarro et al. (2015).

The resulting selection of microwindows (occupation matrix) is shown in Fig. 3. The selected spectral points belong mainly to the lines of the fundamental band in the 60–72 and 102–142 km regions and of the second hot bands in the 75–102 km region. More detailed information on the microwindows used in the retrieval at different altitudes is given in the Supplement.

The retrieval method was applied to all MIPAS UA daytime scans. We considered all scans with a solar zenith angle (SZA) smaller than 90° at the centre-of-scan tangent point. The change in the CO_2 non-LTE populations along the line of sight due to the different solar illumination conditions were

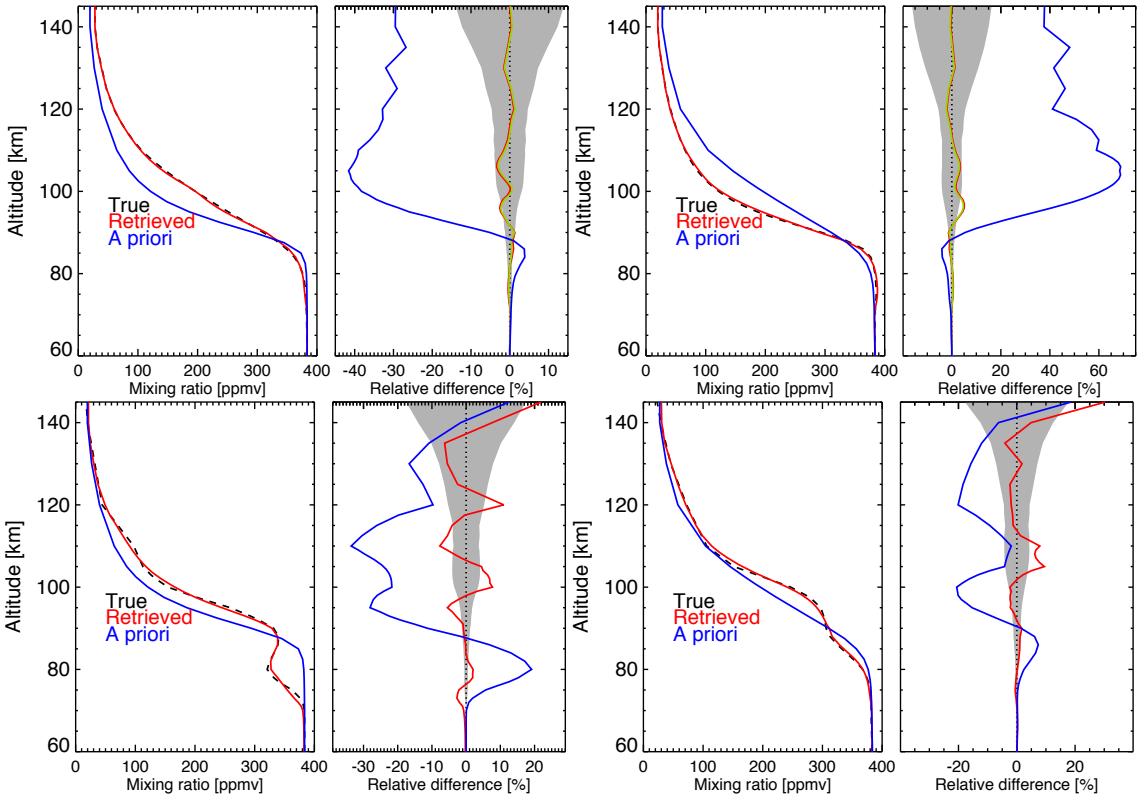

Figure 4. Sensitivity of the retrieved CO_2 profile to the a priori CO_2 profile for several conditions. Upper left panels: for a midlatitude true profile and a polar summer a priori profile. Upper right panels: for a polar summer true profile and a midlatitude a priori profile. Lower left panels: for a true profile extremely low in the upper mesosphere as in Rezac et al. (2015) and a polar summer a priori profile. Lower right panels: for a true profile with an upper mesospheric wave-like perturbation and a midlatitude a priori profile. The relative differences true-retrieved profiles (right panels) are referred to the CO_2/LOS joint retrieval (red solid line) and to the single-parameter CO_2 retrieval (green line, hardly visible, shown only for the midlatitude and polar summer cases, upper row). The blue line is the a priori profile. The shaded area is the noise error of the retrieved profile. Note that the true-retrieved differences (red line) are within the noise error for nearly all altitudes and cases.

taken into account as described by Funke et al. (2009) for the case of CO.

4 Proof of concept of the CO_2-LOS joint retrieval

In order to test the performance of the retrieval set-up we have applied it to synthetic spectra calculated for several atmospheric conditions using the Karlsruhe Optimized and Precise Radiative transfer Algorithm (KOPRA; Stiller et al., 2002) and the GRANADA non-LTE model. We investigate the sensitivity of the retrieval of CO_2 vmr to the CO_2 vmr and LOS a priori profiles separately. In particular we are also interested in knowing if the retrieval yields reasonable results when the CO_2 and LOS a priori profiles are very different from the actual atmospheric and observational conditions.

The tested conditions include, first, the two most common situations we expect to encounter in the retrievals: the midlatitude case, for which we have taken the April 45° N daytime (SZA = 44.5°) reference atmosphere, and the polar summer case for which we have taken the January 75°S (SZA = 58.7°) reference atmosphere (Funke et al., 2012; Jurado-Navarro et al., 2015). We have additionally considered two other cases. One is the rather extreme CO_2 profile that was found by Rezac et al. (2015) in the inversion of SABER radiances (see the top-right panel of their Fig. 12), with very low CO_2 vmr between 70 and 85 km and a pronounced peak near 90 km. The other case was chosen to check if our algorithm would be able to retrieve the expected effect of waves propagation on the CO_2 vmr profile in the upper mesosphere and lower thermosphere. For this latter test, we looked at the variability of CO_2 vmr in the WACCM model at all latitudes, longitudes and local times during a whole year of data co-located with MIPAS measurements and extracted the profile with the largest oscillation (see lower right panel of Fig. 4).

The CO_2 a priori profiles for the four cases described above were taken to substantially differ from the "true" profiles, yet physically feasible. Thus, for the true midlatitude case we took an a priori typical SD-WACCM profile corre-

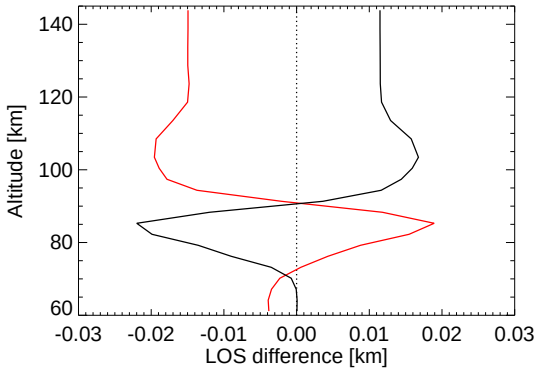

Figure 5. Sensitivity of the retrieved LOS (from the CO_2–LOS joint retrieval) to the CO_2 a priori profile uncertainties for midlatitude (red) and polar summer (black) conditions. The lines show the retrieved–true LOS differences.

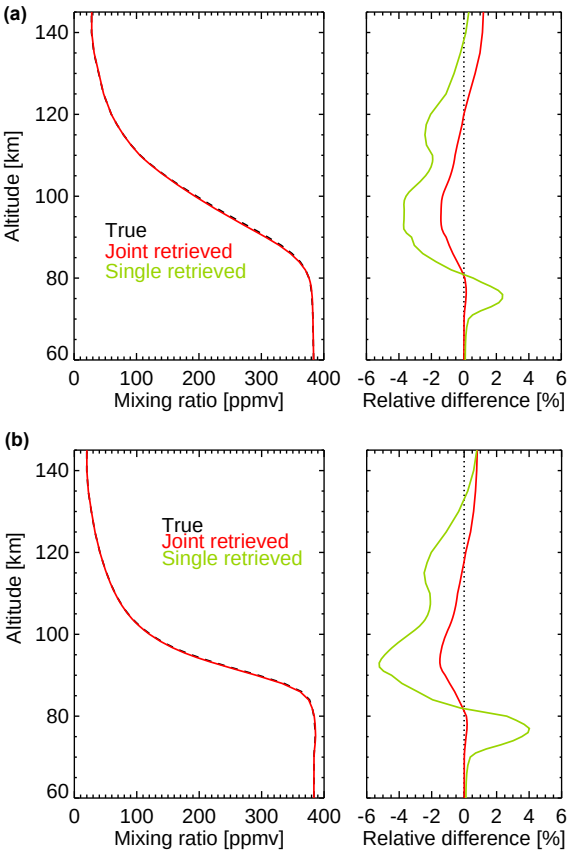

Figure 6. (a) Sensitivity of the retrieved CO_2 to LOS a priori uncertainties for midlatitude conditions. The relative differences (retrieved–true) (right panel) are referred to the joint CO_2-LOS retrieval (red solid line) and to the single-parameter CO_2 retrieval (green line). **(b)** As **(a)** but for polar summer conditions.

sponding to polar summer and, viceversa, for the true polar summer case we took as a priori profile the SD-WACCM profile corresponding to the midlatitudes. For the SABER-like CO_2 true profile we choose the previous SD-WACCM polar summer profile (corresponding to the seasonal conditions where it was found) and, for the wave-like CO_2 true profile, we choose a typical smooth midlatitude profile.

Under midlatitude conditions, the retrieved CO_2 profile differs from the true profile by less than 2–3 % in the whole altitude region (upper left panels in Fig. 4). Compared to the difference with the a priori profile (up to 40 %), the agreement between the retrieved profile and the true one can be considered excellent. It is worth noting that the difference is smaller than the noise error at all altitudes. Regarding polar summer conditions, the differences between the retrieved and the true profiles are generally smaller than 2 % (the a priori profile differs from the true profile up to 60 %) except at 95 to 110 km where the range is 2–4 % (upper right panels in Fig. 4). We also demonstrate that our algorithm would be able to retrieve unusual profiles such as those encountered by Rezac et al. (2015) in the SABER data (lower left panels in Fig. 4). Retrieved minus true differences are generally smaller than 3 %. The only exceptions occur at altitudes where the true profile has abrupt gradients (note the blue line in the relative difference panel) where our algorithm, within its vertical resolution, is not able to fully recover them. Similarly, the lower right panels of Fig. 4 also shows that a wavy CO_2 profile as predicted by WACCM, with a wave amplitude of about 20 %, would be fully recovered by our algorithm.

We have also tested the effect of the a priori CO_2 when retrieving only the CO_2 vmr and keeping the LOS fixed, i.e. with CO_2 as a single-parameter retrieval. The result is shown by the green line in the upper panels of Fig. 4. We see that for both midlatitude and polar summer atmospheric conditions, the differences between the retrieved CO_2 with and without the joint fit of LOS are only marginal. Very similar results are found for the other two cases (not shown). Also, the inspection of the retrieved LOS in the joint fit case (Fig. 5) shows that the mapping of the CO_2 a priori uncertainties on the LOS is very small (less than 20 m).

We also tested the impact of a perturbation of the LOS a priori information on the retrieved CO_2. We applied a sine function perturbation to the LOS with a value of 0 m at 60 and 142 km and a maximum of 200 m at 90 km. Above 90 km, the use of the perturbed a priori LOS profile in the CO_2–LOS joint retrieval introduces deviations of the retrieved CO_2 from the true profile smaller than 1–2 %, while differences are negligible below (see red line in Fig. 6a and b). On the other hand, the application of the perturbed LOS in the single-parameter CO_2 retrieval introduces a significant systematic error of up to 3–4 % for the midlatitudes and an even larger error (up to 5 %) for polar summer above 70 km (see green line in Fig. 6a and b). In Sect. 5.2 we also discuss the effects of using the joint CO_2-LOS or the CO_2-only retrievals on the total systematic error, resulting in a notably larger uncertainty for the CO_2-only retrieval.

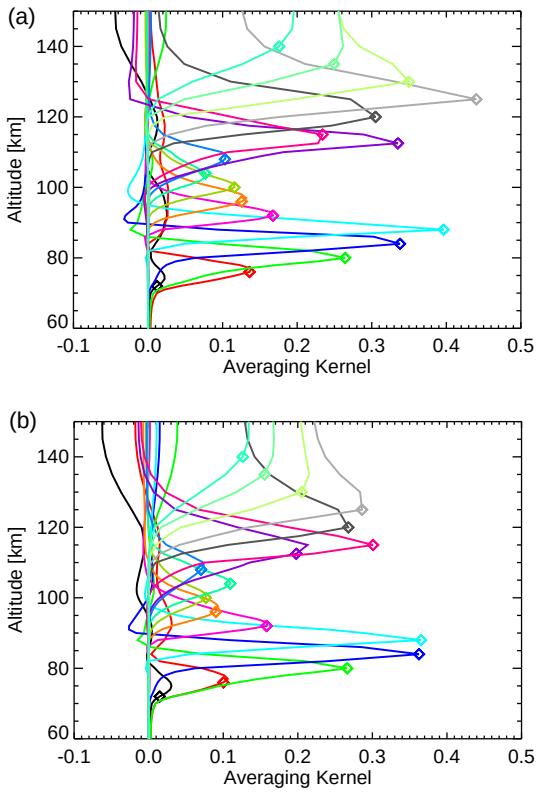

Figure 7. **(a)** Columns of the averaging kernel of the CO_2 vmr from the joint CO_2-LOS retrieval for midlatitude conditions. **(b)** As **(a)** but for polar summer conditions.

Therefore, these results give us confidence in the retrieval scheme and we conclude that the impact of a priori profile uncertainties on the retrieved CO_2 is very small, generally in the $\lesssim$ 1–3 % range. Furthermore, fitting the LOS jointly was found to not degrade the retrieved CO_2 mixing ratios while avoiding important systematic errors due to LOS uncertainties.

Figure 7a and b shows the columns of the averaging kernel (AK) of the CO_2 vmr from the joint CO_2-LOS retrieval at several altitudes for the most common cases of midlatitude and polar summer conditions. Note that the magnitude of the averaging kernel elements responds to both the instrumental sampling (the coarser the sampling the smaller the AK elements) and the retrieval grid (the coarser the grid the larger the AK elements). Since both quantities vary with altitude, regions with different AK magnitudes occur. There are two clear regions with higher sensitivity, one ranging from around 75 to 95 km and another from $\sim$ 105 to 135 km. In the lower region most of the information comes from the second hot bands (as discussed above) and, in the upper region, from the first, mainly fundamental 4.3 µm bands. There is a clear region in between where the sensitivity is smaller. It is also noticeable that, even after the careful selection of the microwindows, it is difficult to obtain information about the CO_2 vmr in the lowermost latitudes, below around 70–75 km. The averaging kernel column corresponding to the lowermost altitude shown in Fig. 7a and b, 72 km, maximizes a few kilometres above this altitude. It also has a negative tail above 120 km, caused by the strong regularization applied to the CO_2 profile at its lower edge in conjunction with an optically thick radiative transfer. The retrieval algorithm responds to a positive perturbation of the CO_2 in the strongly regularized profile range (below 70 km) with a reduction of the thermospheric CO_2 column (i.e. reduction of absorption). Similar features are shown for the averaging kernel columns corresponding to altitudes below 72 km. The decrease of the vertical resolution above $\sim$ 120 km is evident, with the averaging kernels becoming wider, partially due to the coarser measurement sampling.

For a further check of the quality of the retrievals we inspected the residual spectra at several tangent heights (see Fig. 8a and b). These figures show the residuals, not only at the spectral points used in the retrieval of CO_2 (the CO_2 microwindows, red-shaded bands), but also at other wave numbers, which informs us about the accuracy of the used collisional rates of the non-LTE model. In general, the residuals are very small, particularly in the CO_2 microwindows. They still show, however, some systematic differences at wavelengths outside the CO_2 microwindows at lower tangent heights (72 km), but in the order of $\pm$(1–2) nW/(cm^2 sr cm^{-1}), which is only $\sim$ 1 % of the signal. At smaller wave numbers (2280–2320 cm^{-1}), a large fraction of these differences can be attributed to the 4.3 µm fundamental band of second isotopologue (636), for which the collisional rate with N_2(1) was not retrieved by Jurado-Navarro et al. (2015). At higher tangent heights the root mean square (rms) decreases, leading to even better simulations of the measurements, in particular, the radiance of the mentioned isotopic band.

The residuals for the polar summer latitudes (see Fig. 8b) are very similar to those for the midlatitudes, with rms very similar or even slightly smaller at lower tangent heights. At tangent heights of 92 and 102 km, we appreciate some systematic residuals which are more clear than at the midlatitudes, though still very small. These residuals are most likely introduced by a systematic error in the kinetic temperature, distorting the rotational distribution, but could even be caused by rotational non-LTE.

It is important to remark that the residuals in the whole spectral range shown here, as a result of the inversion of CO_2, are nearly identical to those obtained in the retrieval of the collisional rates (compare Fig. 8a and b with Fig. 8 in Jurado-Navarro et al., 2015). Also note that the residuals in the CO_2 microwindows (red-shaded areas) are generally smaller than at other wave numbers of this spectral region.

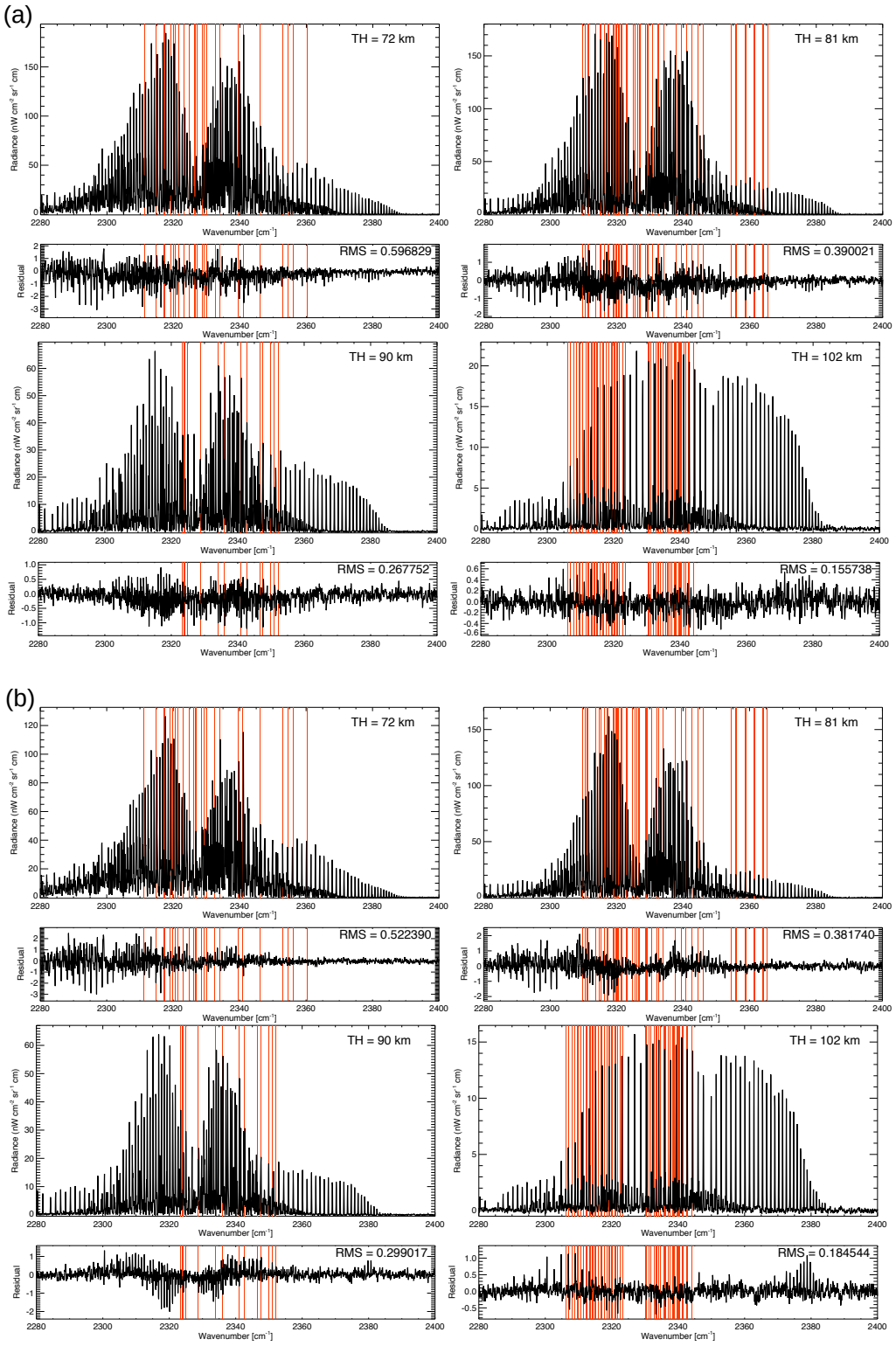

Figure 8. **(a)** Co-added measured spectra (upper panels) and residuals, simulated-measured (lower panels), in the whole 4.3 µm spectral region at tangent heights of 72, 81, 90 and 102 km obtained from the retrievals of CO_2 for 30 March 2010 averaged in the 40° S–40° N latitude range. Over-plotted in reddish are the microwindows used in the retrieval of CO_2 at each altitude (see Fig. 3). The residuals are in the same units as radiances. Note the different scales for the different altitudes. The root mean square (rms) of the residuals for the whole spectral range are also given. **(b)** As **(a)** but for polar summer conditions. The average was taken over the 142 scans available for 17 January 2010 in the 80–40° S latitude range.

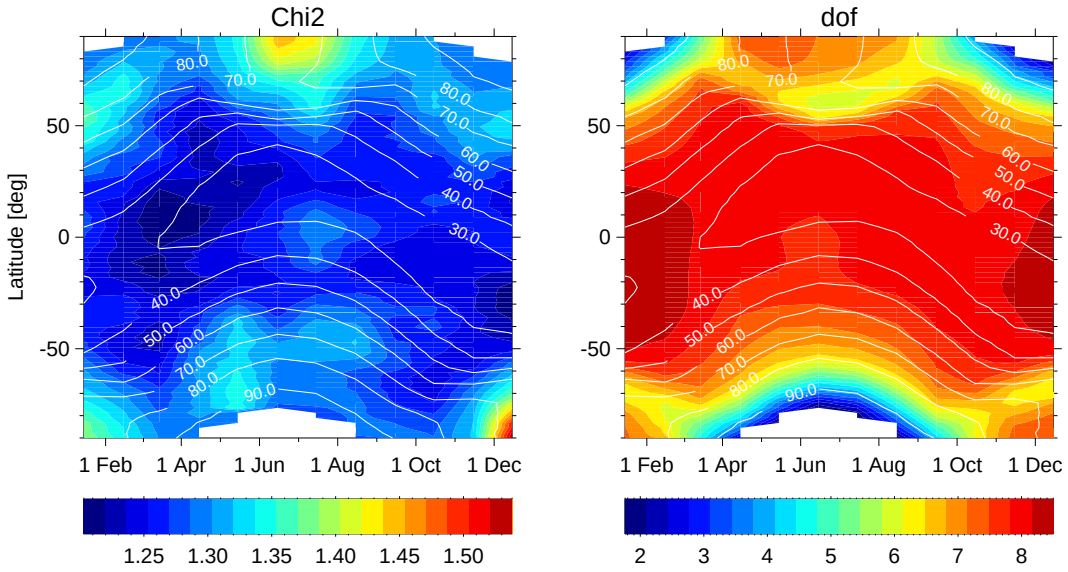

Figure 9. Latitude-seasonal distributions of the χ^2 of the residuals (left) and of the number of degrees of freedom of the retrieved CO_2 vmr (right) for the 2010–2011 period. Over-plotted on the distributions is the solar zenith angle (SZA) in degrees with white lines.

5 Characterization of the retrieved CO_2 vmr

To give the reader a general view on the quality of the retrieved CO_2 profile we show in Fig. 9 the latitudinal and seasonal dependencies of χ^2 of the residuals and the number of degrees of freedom of the retrieved CO_2 for the 2010–2011 period. The solar zenith angle is over-plotted on those distributions. The χ^2 is generally smaller than 1.3 but reaches larger values (up to about 1.5) at very high latitudes in the polar summer. The number of degrees of freedom generally ranges between 7 and 8 for solar zenith angles smaller than 80°. For solar zenith angles in the range of 80–90° it is reduced to 4–6.

5.1 Precision and vertical resolution

The vertical resolution and the precision are two important parameters for characterizing the quality of any retrieval. The vertical resolution is estimated by the full width at half maximum of the rows of the averaging kernel matrix. Figure 10 shows the zonal means of these parameters calculated from the retrieved data from MIPAS measurements in the UA mode for 2010 and 2011 for each season corresponding to the following months: December–January–February, March–April–May, June–July–August and September–October–November. The zonal mean CO_2 distribution is also shown (left column) for reference.

In general, the precision varies with altitude ranging from ~ 1 % below 90 km, 5 % around 120 km and larger than 10 % above 130 km. The larger values at higher altitudes are due to the lower signal-to-noise ratio. There are some latitudinal and seasonal variations, which are driven mainly by the solar illumination conditions.

The vertical resolution is typically around 5–7 km below 120 km. Above that altitude, it is coarser, with values larger than 10 km, mainly caused by the coarser vertical sampling (5 instead of 3 km) of the measured spectra. Around ~ 105 km, a slight degradation of the vertical resolution is observed. This altitude corresponds to the tangent height region where the microwindows include lines from the second hot bands only while the fundamental band lines are used above. The latter, as discussed above in Sect. 3, are still rather optically thick at these tangent heights and hence have been rejected.

5.2 Systematic errors

The systematic errors were estimated from the retrieval response to perturbations in the spectra of the following parameters: pressure/temperature, $O(^1D)$ and $O(^3P)$ abundances, MIPAS gain calibration and solar flux. The magnitudes of these perturbations are the same as those used in the retrieval of the collisional rates in Jurado-Navarro et al. (2015) and were already present. There are, however, two exceptions, the temperature, which was assumed with larger errors above 100 km, and the LOS, which was retrieved here and hence its error is already included in the error of the retrieved CO_2. Following Jurado-Navarro et al., for temperature we assumed retrieval errors reported by García-Comas et al. (2014) and Bermejo-Pantaleón et al. (2011), which take values of 1 K from 50 to 70 km, 2 K between 70 and 80 km, 5 K between 80 and 100 km, 10 K between 100 and 110 km and 15 K between 110 and 142 km for midlatitude conditions. In the case of the polar summer the errors in the 85–100 km altitude range are significantly larger. For those conditions we included values of 4, 4, −5, −15, −20, 8 and 15 K for altitudes of 80, 85, 90,

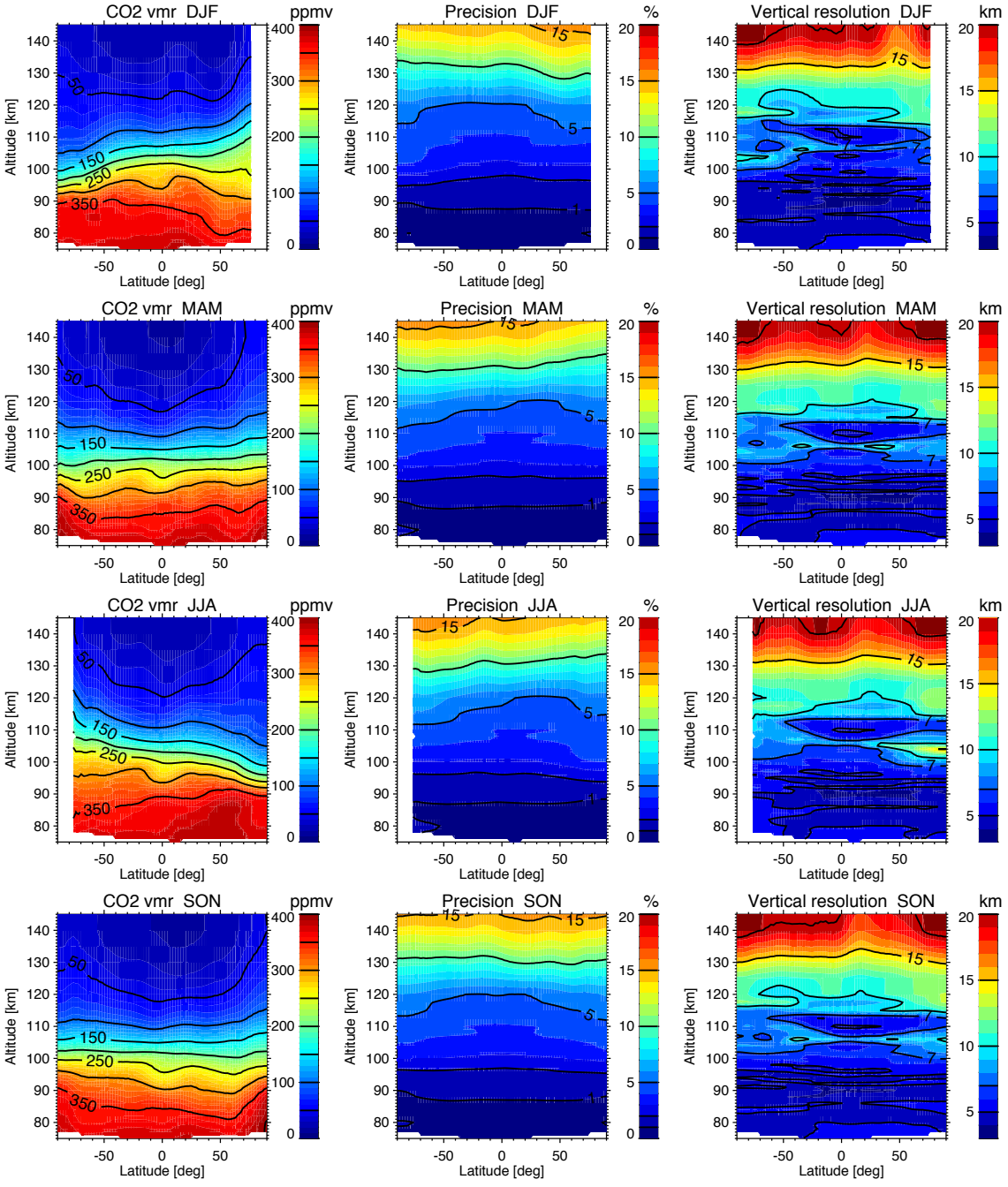

Figure 10. Latitude-altitude cross sections of CO_2 vmr (left column), precision (centre column) and vertical resolution (right column). The rows, from top to bottom, correspond to the boreal winter (DJF: December–January–February), the vernal equinox (MAM: March–April–May), the austral winter (JJA: June–July–August) and the autumnal equinox (SON: September–October–November). The MIPAS data include the measurements taken in 2010 and 2011 in the UA mode.

95, 100, 110 and ≥ 120 km respectively. Note the change of sign with altitude introduced by the non-LTE errors.

Rezac et al. (2015) used a joint CO_2-temperature retrieval in the analysis of SABER data. Such a retrieval would use a more consistent approach than the joint CO_2-LOS retrieval in the case of MIPAS (below 100 km) since it would allow us to diminish the mapping of temperature errors into CO_2 errors, though it is more computationally expensive. We have estimated how much the CO_2 vmr would be improved in a joint CO_2-temperature retrieval, taking the error analysis of MIPAS temperature carried out by García-Comas et al. (2012) as a basis. In that analysis the effects

of the hydrostatical adjustment of pressure due to the temperature changes were taken into account. We only consider the altitudes below 100 km, where the temperature retrieved from the CO_2 15 µm MIPAS spectra is used, and hence the CO_2 vmr is needed. In the best case, assuming the CO_2 vmr is free of errors in the temperature retrieval, the temperature error would be improved for midlatitude conditions in about 1 K at 85 km and 0.8 K and 0.1 K at 90 and 100 km respectively (see Table 2 in García-Comas et al., 2012). For polar summer conditions, the reduction is smaller, 0.7 K at 85 km and 0.1 K at 90–100 km, because non-LTE errors are more relevant. These errors would improve the retrieved CO_2 error in 0.7 % at 85 km and only 0.1 % at 90–100 km for the midlatitudes. For polar summer latitudes, the improvements would be even smaller because, at 85 km, the temperature error contribution to the CO_2 error budget is smaller (see Table 1) and, at higher altitudes, because the improvement in the temperature error is not significant. Hence, we expect that the joint CO_2-temperature retrieval would not significantly improve the accuracy of the retrieved CO_2 vmr.

Regarding the error introduced by the absolute pointing (the error due to the relative pointing, i.e. between adjacent scans, is already included in the retrieval error since it is jointly retrieved with the CO_2 vmr), von Clarmann et al. (2003) estimated the total systematic error in the retrieved absolute pointing from 15 µm to be less than 200 m. This error introduces an error in the CO_2 vmr that is smaller than 1 % below 90 km, between 1 and 1.5 % at 90–120 km and smaller than 1 % above that altitude. Overall this error is negligible in comparison with the other error sources (see Table 1).

For the atomic oxygen we assumed an uncertainty of 50 %. In view of the recent measurements of $O(^3P)$ by different instruments (see e.g. Kaufmann et al., 2014; Zhu et al., 2015; von Savigny and Lednyts'kyy, 2013; Mlynczak et al., 2013) it might be somehow underestimated. However, uncertainty estimates in this range have been used for the inversion of temperature from SABER measurements (Remsberg et al., 2008) and from MIPAS spectra (García-Comas et al., 2012, 2014), where the impact of $O(^3P)$ is larger than in the retrieval of CO_2; and larger in the retrieval of CO_2 from SABER radiances in the same spectral region (4.3 µm) than used here (Rezac et al., 2015). Furthermore, an even smaller error (20 %) has been used in the derivation of the k_{CO_2-O} collisional rate, where the $O(^3P)$ error has a larger impact since it directly propagates into the collisional rate (Feofilov et al., 2012). Thus, in order to make the error budget comparable with other recent measurements we decided to adopt the same uncertainty of 50 %.

The uncertainty in $O(^1D)$ has been considered with different values below about 80 km, where the major production comes from photo-dissociation of O_3, and above that altitude, where it is mainly produced by the photo-dissociation of O_2. In the stratosphere and lower mesosphere we used the O_3 retrieved from simultaneous MIPAS spectra which has an uncertainty of about 10–15 % (Smith et al., 2013; Glatthor et al., 2006). Since the photochemical reaction is well known we considered an upper limit error of O_3, 15 % for the $O(^1D)$. Above 80 km, the comparison of the photochemical model of Funke et al. (2012) with the independent model of González-Galindo et al. (2005) give differences smaller than 2 % at all altitudes. Also, the pressure/temperature has been measured with an mean error of about 15 K (see above) and the error of the O_2 vmr from the NRLMSIS-00 model is rather small. Therefore, the assumed error of 30 % seems realistic. The other perturbations, which are discussed in detail in Jurado-Navarro et al. (2015), are 1.25 % for the gain calibration and 1 % for the solar flux.

In addition, systematic CO_2 retrieval errors due to uncertainties in the collisional rates used in the non-LTE modelling need to be taken into account. However, since the CO_2 collisional parameters used here in the CO_2 inversion have been retrieved from MIPAS measurement in the same spectral region (see Jurado-Navarro et al., 2015), the CO_2 retrieval errors due to systematic errors of the retrieved rates are expected to be correlated with the errors caused by model parameter uncertainties. Therefore, adding the systematic er-

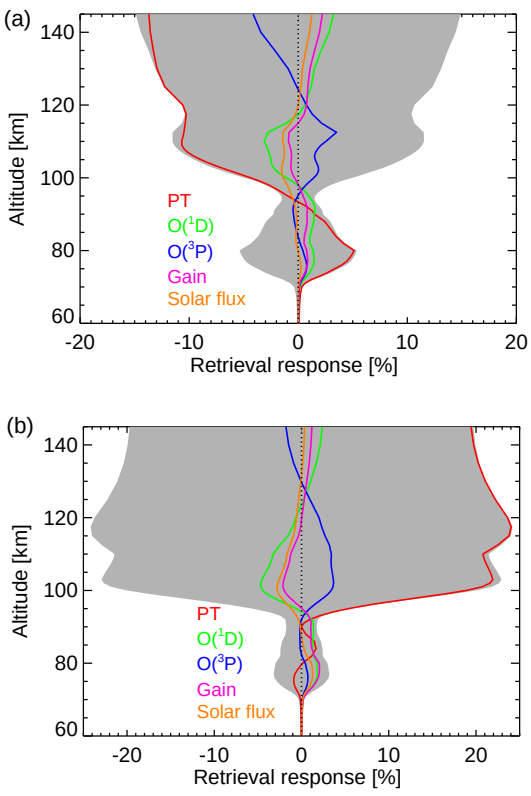

Figure 11. **(a)** Systematic errors of the CO_2 vmr introduced by different error sources for midlatitude conditions. CO_2 retrieval responses to individual model parameter perturbations (reflecting their estimated uncertainties) are shown by the coloured lines. The shaded area represents the total systematic error. **(b)** As **(a)** but for polar summer conditions.

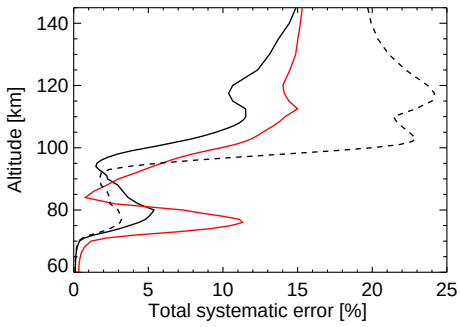

Figure 12. Total systematic errors of the main atmospheric parameters from the joint CO_2-LOS (black solid line) and CO_2-only (red line) retrievals for midlatitude conditions. The dashed black line shows the total systematic error of the joint CO_2-LOS retrieval for polar summer. The total errors are calculated from the quadratic sum of the retrieval responses to individual model parameter perturbations shown in Figs. 11a and b.

rors due to collisional rate uncertainties quadratically to the other errors would not be adequate. For instance, it might occur that an overestimation of the solar flux introduces a low bias of a certain collisional rate, but the use of the underestimated rate in the CO_2 retrieval compensates the "direct" CO_2 error caused by assuming a solar flux that is too low. Therefore we calculate the $\Delta CO_2(y_i)$ error due to a given model parameter, y_i, i.e. pressure/temperature, $O(^1D)$, $O(^3P)$, gain calibration and solar flux, by means of

$$\Delta CO_2(y_i) = \left(\frac{\delta CO_2}{\delta y_i}\right)_{\forall x_j = cte} \Delta y_i + \sum_j \left(\frac{\delta CO_2}{\delta x_j}\right) \Delta x_j(y_i),$$
$$\text{with } \Delta x_j(y_i) = \left(\frac{\delta x_j}{\delta y_i}\right) \Delta y_i, \quad (2)$$

where the second term on the right-hand side accounts for the propagation of the error of model parameters, y_i, through the errors in the retrieved collisional parameters, $\Delta x_j(y_i)$. The sum extends over the retrieved collisional parameters, x_j: k_{vv2}, k_{vv3}, k_{vv4}, k_{F1}, k_{F2} and f_{vt}, which have errors due to the model parameters y_i, $\Delta x_j(y_i)$ listed in Table 3 of Jurado-Navarro et al. (2015). The first term on the right-hand side, where Δy_i is the error of model parameter y_i, has been discussed above. The total systematic error in CO_2 is then calculated by a quadratic sum over the errors of all model parameters, $\Delta CO_2^{\text{Total}} = \sqrt{\sum_i [\Delta CO_2(y_i)]^2}$. The resulting corrected retrieval responses to the model parameter perturbations (reflecting their estimated uncertainties) are shown in Fig. 11a and b and are listed in Table 1 for some altitudes.

The calculations indicate that the largest error contribution above 100 km comes from the pressure/temperature uncertainties for both considered atmospheric conditions, reaching values up to ∼ 15–16 % in midlatitude conditions (Fig. 11a) and ∼ 20 % in polar summer conditions (Fig. 11b). Below, the pressure/temperature error maximizes again around 80 km, with maximum values at midlatitude conditions of up to ∼ 4 %. The MIPAS gain calibration and solar flux uncertainties introduce errors of 2–3 % from 85 up to 110 km in both conditions. The total error below 90 km in polar summer conditions is indeed dominated by these uncertainties. The $O(^1D)$ and $O(^3P)$ uncertainties have a non-negligible contribution above 95 km with the largest values up to 4 % at 105 km in polar summer conditions.

It is important to highlight that, in polar summer conditions, the MIPAS temperature retrieved from the NO 5.3 µm emission is smaller than MSIS (Mass Spectrometer and Incoherent Scatter) temperatures in up to 10 K in the lower thermosphere (Bermejo-Pantaleón et al., 2011). Thus, the use of thermospheric MIPAS temperature, instead of MSIS, increases the retrieved CO_2 vmr by up to 15 % under these particular conditions.

Regarding the effects of the joint CO_2-LOS retrieval on the total systematic error, Fig. 12 shows that it is notably larger for the CO_2-only retrieval than for the joint CO_2-LOS retrieval. This indicates that a large fraction of the spectral residuals due to the systematic errors of the different parameters is compensated by the LOS in the joint retrieval while in the CO_2-only retrieval all errors map onto the CO_2 vmr profile. In this sense, the joint CO_2-LOS retrieval is also useful for dampening systematic errors of the retrieved CO_2 vmr.

Deviations of the retrieved profile from the true profile when perturbing the a priori profile are often called smoothing errors. However, while it is important to assess the sensitivity of the retrieval to the a priori profile shape as we do above, we do not include smoothing errors in the overall error budget. Firstly, because the concept of "smoothing errors" itself is questionable (von Clarmann, 2014) and, secondly, because these deviations can be implicitly accounted for in comparisons to model simulations or independent observations by applying the MIPAS averaging kernels to the latter.

One important result that should be mentioned is that the systematic errors obtained here in the retrieved CO_2 vmr are much smaller than those obtained before in previous measurements of CO_2 using limb emission measurements of the 4.3 µm atmospheric radiance (e.g. López-Puertas et al., 1998; Kaufmann et al., 2002; Rezac et al., 2015). The main reasons are as follows. Firstly, more accurate non-LTE collisional rates have been used, enabled by the high-resolution MIPAS spectra (see Jurado-Navarro et al., 2015). Secondly, the wide spectral range, together with the high spectral resolution of MIPAS, has allowed the retrieval of the temperature and O_3 up to about 100 km, and the temperature in the lower thermosphere (up to ∼ 170 km) before the CO_2 vmr. The use of these concentrations has significantly reduced the systematic error of CO_2.

We have also considered the errors introduced by other possible non-LTE processes. One mechanism operating in

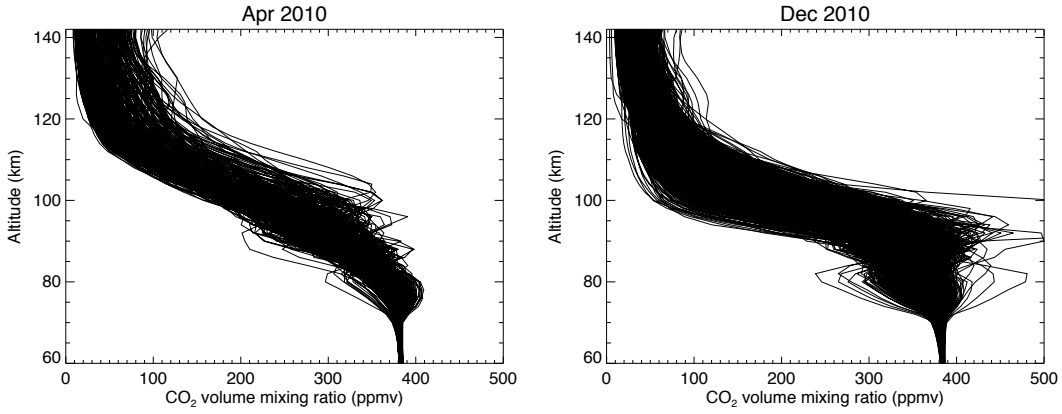

Figure 13. Examples of the CO_2 vmr profiles measured by MIPAS during 2010 for April (equinox, left) and December (solstice, right).

the auroral region is the excitation of $CO_2(v_3)$ via $V - V$ energy transfer from $N_2(v)$ which is excited by auroral electrons. However, its importance during daytime conditions seems to be negligible, much smaller than the solar absorption at 4.3 and 2.7 µm since SABER CO_2 4.3 µm radiance measurements show that the daytime signal is more than 2 orders of magnitude larger than the night-time signal in the auroral regions.

The possible excitation of CO_2 by "hot" O atoms was postulated by Feofilov et al. (2012) as an additional source of the excitation of $CO_2(v_2)$ (15 µm) in order to understand the differences between the collisional rates of CO_2-O measured in the laboratory and those derived from atmospheric measurements. Sharma (2015) found, however, that the chance of a hot atom colliding with CO_2 is virtually nil in the mesosphere and lower thermosphere. The excitation of CO_2 in the more energetic v_3 state would then be even less probable. Thus, as there is no evidence of such excitation mechanism for $CO_2(v_3)$, its inclusion is not justified. We should also note that this mechanism was not included in the recent retrieval of CO_2 from SABER measurements (Rezac et al., 2015).

In this work we have not included rotational non-LTE. Based on previous assessments (Gusev, 2002), rotational non-LTE in the $CO_2(v_3)$ ro-vibrational states (emitting in the fundamental band used here in the retrieval of CO_2 above 100 km, where rotational non-LTE has a larger propensity to occur) is likely to introduce only marginal errors in the vertical range of interest (70–140 km), being negligible compared to other error sources.

6 MIPAS CO_2 climatology for 2010–2011

Figure 14a and b shows the monthly zonal mean CO_2 vmr retrieved from MIPAS daytime spectra taken in its upper atmosphere (UA) mode. The figure shows the major features expected for the CO_2 distribution and predicted by models. Compare, for example, the CO_2 zonal mean distributions obtained by the CMAM model for April and August (middle panel of the upper row in Fig. 3 and top-right panel in Fig. 8 in Beagley et al., 2010), with the corresponding months in Fig. 14a and b. Also the similar broad features are shown by the WACCM-SD model simulations (see the upper panels of Fig. 3 in Garcia et al., 2014 for February and April). Those features comprise the abrupt decline of the CO_2 vmr above around 80–90 km. The other major feature is the seasonal change of the latitudinal distribution, leading to higher CO_2 vmr from 70 up to $\sim$ 95 km in the polar summer, induced by the ascending branch of the mean circulation, and lower CO_2 abundances, with respect to the tropics and polar summer, at the same altitudes in the polar winter region. It is noticeable that the distribution reverses above $\sim$ 95 km, CO_2 being more abundant in the polar winter region than at the midlatitudes and polar summer; also as a consequence of the reversal of the mean circulation (see e.g. Smith et al., 2011). The solstice seasonal distribution, with a significant pole-to-pole CO_2 gradient lasts about 2.5 months in each hemisphere (November to February and May to August), while the seasonal transition occurs quickly, mainly in April and October.

Another observed feature is the rapid increase of CO_2 vmr from mid-high latitudes towards the polar regions in the lower thermosphere during the equinoxes (more evident in April and October). We cannot find any physical reason for it and we do not discard that this could be a retrieval artefact caused by the inversion of CO_2 in conditions of very high ($> 80°$) solar zenith angles.

A comparison of the MIPAS CO_2 vmr with ACE measurements for 4 days (two in solstice and two in equinox) have been presented in Jurado-Navarro et al. (2015), showing a good general agreement. A more detailed comparison with ACE data covering a more extended period as well as with SABER observations and with WACCM simulations is to be presented in a future work.

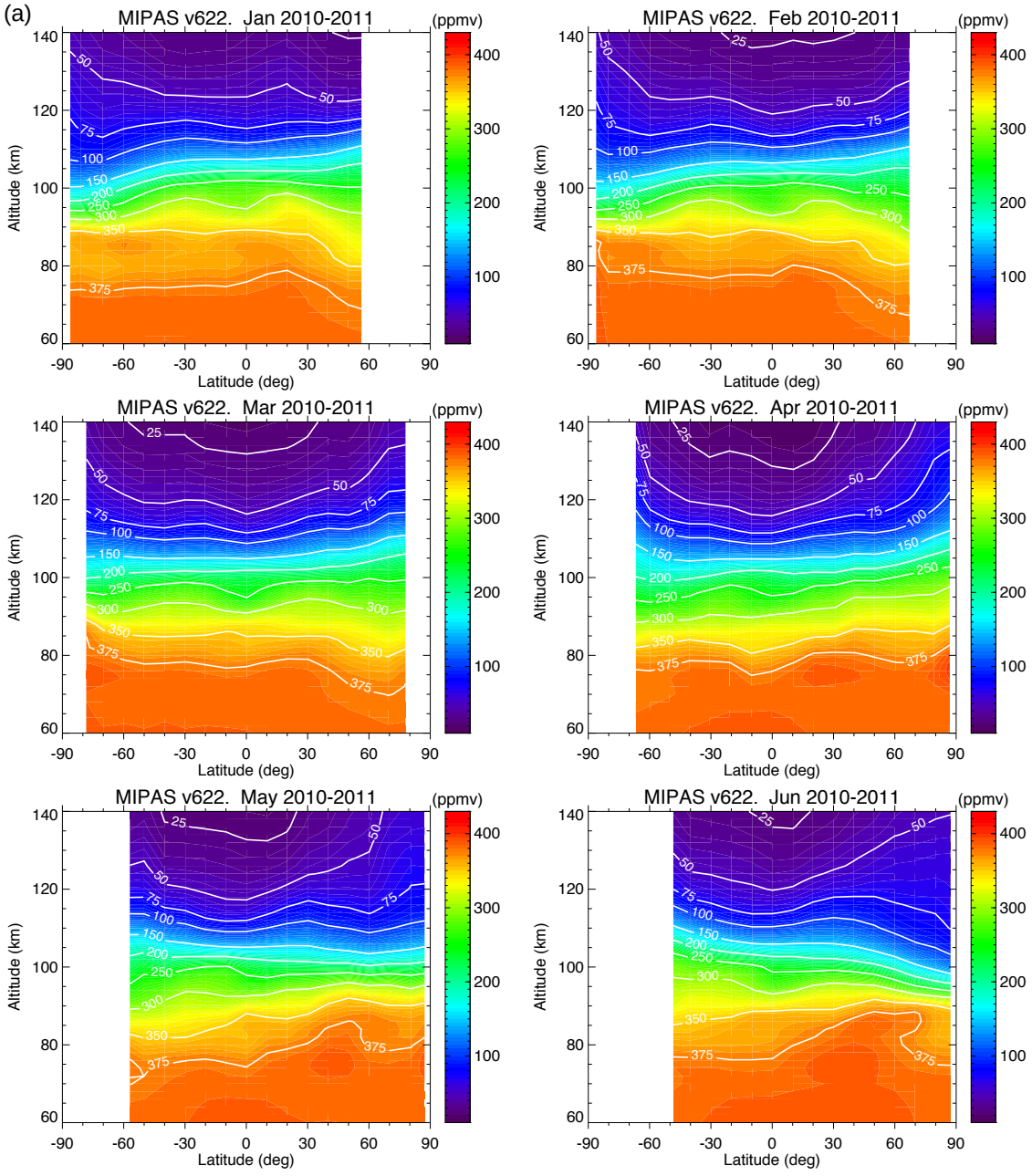

Figure 14.

7 Conclusions

We have retrieved global distributions of the CO_2 vmr (volume mixing ratio) in the mesosphere and thermosphere (from 70 up to ~ 140 km) for MIPAS daytime high-resolution spectra. This is the first time that the relative CO_2 concentration (vmr, not the CO_2 number density) has been retrieved in the mid-thermosphere (120–140 km). The retrieved CO_2 has an improved accuracy because of the new rate coefficients recently derived from MIPAS (Jurado-Navarro et al., 2015), and the simultaneous MIPAS measurements of other key atmospheric parameters (retrieved in previous steps) needed for the non-LTE modelling like the temperature in the mesosphere and in the thermosphere, as well as the O_3 concentration. In addition, the high spectral resolution of MIPAS allows for an optimized selection of the spectral points (optically thin and moderate points of the lines of the bands) containing the largest amount of information at the different tangent heights, which constrains the retrieval better than an integral wideband radiance measurement.

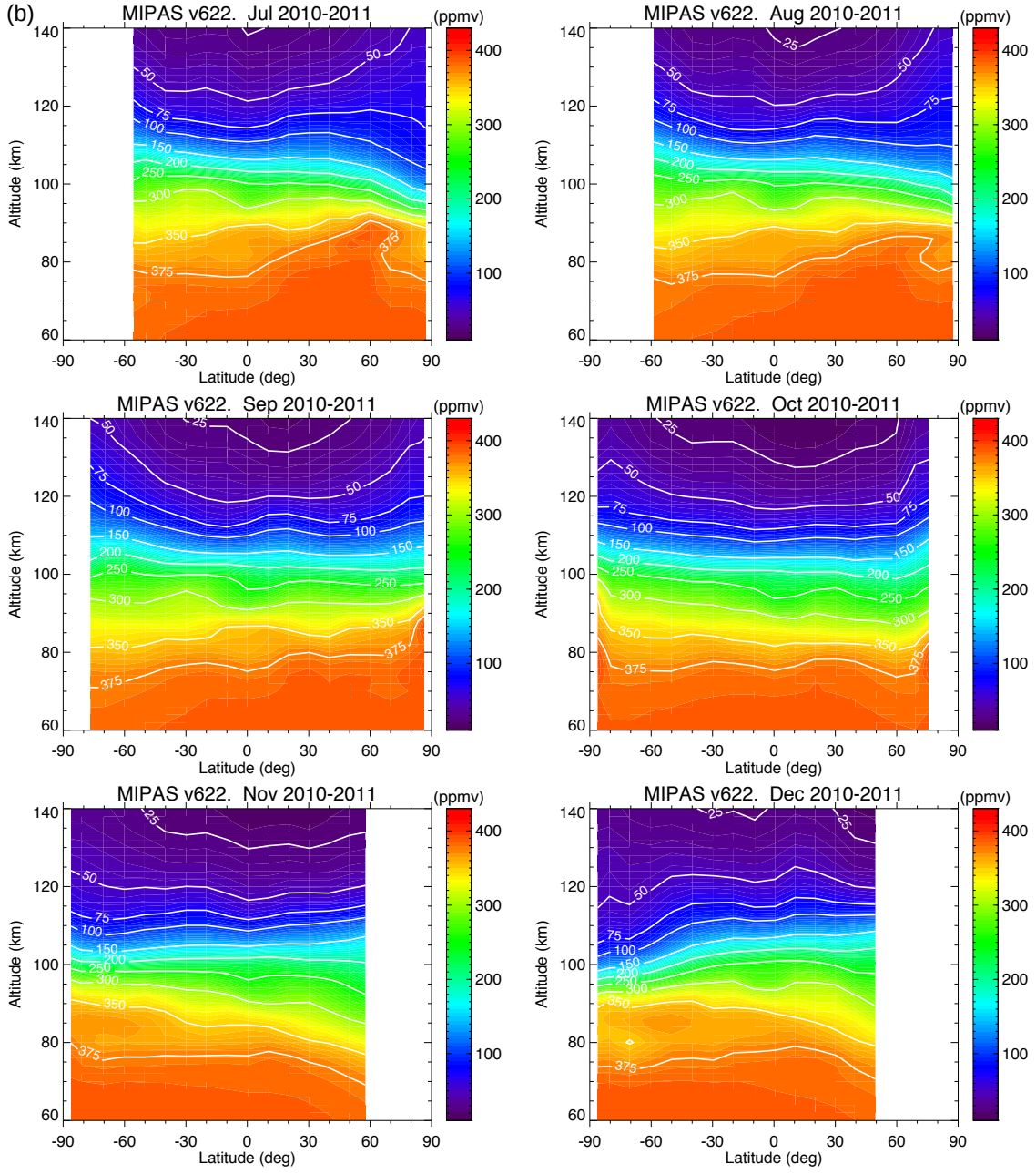

Figure 14. **(a)** Monthly zonal mean CO_2 vmr measured by MIPAS during the 2010–2011 period for the UA mode for months of January to June. **(b)** As **(a)** but for months of July to December.

The CO_2 vmrs have been retrieved using MIPAS daytime limb emission spectra from the 4.3 µm region in its upper atmosphere (UA) mode (data version v5r_CO2_622). Nighttime spectra were not used because they are very noisy and the non-LTE processes operating at night are not known very accurately. The retrieved CO_2 covers from 70 km up to about 140 km and all latitudes except in the dark regions of the polar winter. The inversion of CO_2 has been performed jointly with the line of sight (LOS) by using a non-LTE retrieval scheme developed at IAA/IMK. It takes advantage of other (simultaneous) MIPAS measurements of atmospheric parameters (retrieved in previous steps), such as the kinetic temperature (up to $\sim$ 100 km) from the CO_2 15 µm region, the thermospheric temperature from the NO 5.3 µm, the O_3 measurements (up to $\sim$ 100 km), which allows a strong constraint on the $O(^1D)$ concentration below $\sim$ 100 km, and an accurate calculation of $O(^1D)$ above $\sim$ 100 km. The non-LTE model incorporates the more accurate vibrational–vibrational and

vibrational–translational collisional rates retrieved from the MIPAS spectra.

The precision of the retrieved CO_2 vmr profiles varies with altitude, ranging from $\sim 1\,\%$ below 90 km to 5 % around 120 km and larger than 10 % above 130 km. The larger values at higher altitudes are due to the lower signal-to-noise ratio. There are very few latitudinal and seasonal variations of the precision, which are mainly driven by the solar illumination conditions. The retrieved CO_2 profiles have a vertical resolution of about 5–7 below 120 km and between 10 and 20 at 120–140 km.

Retrieval simulations performed with synthetic spectra have demonstrated that the developed CO_2-LOS joint retrieval allows for a retrieval of the CO_2 profile in the 70–140 km range with high accuracy. The use of strongly perturbed a priori CO_2 and LOS information results in very small different between the true and the retrieved profiles, generally smaller than 2–3 % in the midlatitudes and smaller than 2 % (except near 95–110 km where it ranges at 2–4 %) for polar summer conditions. We have also proven that the algorithm is capable of retrieving unusual CO_2 profiles such as those showing a low vmr between 70 and 85 km and a pronounced peak near 90 km, and also CO_2 profiles affected by wave propagation. The retrieval scheme clearly discriminates the information of CO_2 concentration from the LOS. The mapping of typical CO_2 a priori uncertainties on the LOS is very small (less than 20 m), and a deviation in the a priori LOS profile of 200 m introduces a change in the retrieved CO_2 profile smaller than 1–2 %. We have also found that the systematic errors are significantly reduced when using the CO_2-LOS joint retrieval instead of the CO_2-only scheme.

The major systematic error source is the uncertainty of the pressure/temperature profiles, retrieved also from MIPAS spectra, near 15 µm below 100 km (García-Comas et al., 2014) and from 5.3 µm above 100 km Bermejo-Pantaleón et al. (2011). They can induce a systematic error at midlatitude conditions of up to 15 % above 100 km (20 % for polar summer conditions) and of $\sim 5\,\%$ around 80 km. The systematic errors due to uncertainties of the $O(^1D)$ and $O(^3P)$ profiles are within 3–4 % in the 100–120 km region. The errors due to uncertainties in the gain calibration and in the solar flux at 4.3 and 2.7 µm are within $\sim 2\,\%$ at all altitudes.

The most important features observed on the retrieved CO_2 can be summarized as follows:

- The retrieved CO_2 shows the major general features expected and predicted by models: the abrupt decline of the CO_2 vmr above 80–90 km, caused by the predominance of the molecular diffusion and the seasonal change of the latitudinal distribution. The latter is reflected by higher CO_2 abundances in polar summer from 70 km up to ~ 95 km and lower CO_2 vmr in the polar winter, both induced by the ascending and descending branches of the mean circulation respectively. Above ~ 95 km, CO_2 is more abundant in the polar winter than at the midlatitudes and polar summer regions, caused by the reversal of the mean circulation in that altitude region.
- The solstice seasonal distribution, with a significant pole-to-pole CO_2 gradient lasts about 2.5 months in each hemisphere (November to February and May to August), while the seasonal transition occurs quickly, mainly in April and October.

8 Data availability

The retrieved CO_2 volume mixing ratio data version v5r_CO2_622 will be made available at the IMK-IAA MIPAS data set website: https://www.imk-asf.kit.edu/english/308.php, once the final processing is finished.

The Supplement related to this article is available online at doi:10.5194/amt-9-6081-2016-supplement.

Acknowledgements. The IAA team was supported by the Spanish MCINN under grant ESP2014-54362-P and EC FEDER funds. Maya García-Comas was financially supported by the Ministry of Economy and Competitiveness (MINECO) through its "Ramón y Cajal" subprogramme. The authors acknowledge ESA for providing MIPAS L1b spectra.

Edited by: S. Kirkwood
Reviewed by: A. Feofilov and one anonymous referee

References

Beagley, S. R., Boone, C. D., Fomichev, V. I., Jin, J. J., Semeniuk, K., McConnell, J. C., and Bernath, P. F.: First multi-year occultation observations of CO_2 in the MLT by ACE satellite: observations and analysis using the extended CMAM, Atmos. Chem. Phys., 10, 1133–1153, doi:10.5194/acp-10-1133-2010, 2010.

Bermejo-Pantaleón, D., Funke, B., Lopez-Puertas, M., García-Comas, M., Stiller, G. P., von Clarmann, T., Linden, A., Grabowski, U., Höpfner, M., Kiefer, M., Glatthor, N., Kellmann, S., and Lu, G.: Global Observations of Thermospheric Temperature and Nitric Oxide from MIPAS spectra at 5.3 µm, J. Geophys. Res., 116, A10313, doi:10.1029/2011JA016752, 2011.

De Laurentis, M.: Planning of MIPAS new special modes January 2005 Campaign, Tech. rep., ESA Technical Note, ENVI-SPPA-EOPG-TN-05-0002, 2005.

Feofilov, A. G., Kutepov, A. A., She, C.-Y., Smith, A. K., Pesnell, W. D., and Goldberg, R. A.: $CO_{2(v2)}$-O quenching rate coefficient derived from coincidental SABER/TIMED and Fort Collins lidar observations of the mesosphere and lower thermosphere, Atmos. Chem. Phys., 12, 9013–9023, doi:10.5194/acp-12-9013-2012, 2012.

Fischer, H., Birk, M., Blom, C., Carli, B., Carlotti, M., von Clarmann, T., Delbouille, L., Dudhia, A., Ehhalt, D., Endemann, M., Flaud, J. M., Gessner, R., Kleinert, A., Koopman, R., Langen, J., López-Puertas, M., Mosner, P., Nett, H., Oelhaf, H., Perron, G., Remedios, J., Ridolfi, M., Stiller, G., and Zander, R.: MIPAS: an instrument for atmospheric and climate research, Atmos. Chem. Phys., 8, 2151–2188, doi:10.5194/acp-8-2151-2008, 2008.

Foucher, P. Y., Chédin, A., Armante, R., Boone, C., Crevoisier, C., and Bernath, P.: Carbon dioxide atmospheric vertical profiles retrieved from space observation using ACE-FTS solar occultation instrument, Atmos. Chem. Phys., 11, 2455–2470, doi:10.5194/acp-11-2455-2011, 2011.

Funke, B., López-Puertas, M., Stiller, G. P., von Clarmann, T., and Höpfner, M.: A new non–LTE Retrieval Method for Atmospheric Parameters From MIPAS–ENVISAT Emission Spectra, Adv. Space Res., 27, 1099–1104, doi:10.1016/S0273-1177(01)00169-7, 2001.

Funke, B., López-Puertas, M., García-Comas, M., Stiller, G. P., von Clarmann, T., Höpfner, M., Glatthor, N., Grabowski, U., Kellmann, S., and Linden, A.: Carbon monoxide distributions from the upper troposphere to the mesosphere inferred from 4.7 µm non-local thermal equilibrium emissions measured by MIPAS on Envisat, Atmos. Chem. Phys., 9, 2387–2411, doi:10.5194/acp-9-2387-2009, 2009.

Funke, B., López-Puertas, M., García-Comas, M., Kaufmann, M., Höpfner, M., and Stiller, G. P.: GRANADA: a Generic RAdiative traNsfer AnD non-LTE population Algorithm, J. Quant. Spectrosc. Ra., 113, 1771–1817, doi:10.1016/j.jqsrt.2012.05.001, 2012.

Garcia, R. R., López-Puertas, M., Funke, B., Marsh, D. R., Kinnison, D. E., Smith, A. K., and González-Galindo, F.: On the distribution of CO_2 and CO in the mesosphere and lower thermosphere, J. Geophys. Res.-Atmos., 119, 5700–5718, doi:10.1002/2013JD021208, 2014.

García-Comas, M., Funke, B., López-Puertas, M., Bermejo-Pantaleón, D., Glatthor, N., von Clarmann, T., Stiller, G., Grabowski, U., Boone, C. D., French, W. J. R., Leblanc, T., López-González, M. J., and Schwartz, M. J.: On the quality of MIPAS kinetic temperature in the middle atmosphere, Atmos. Chem. Phys., 12, 6009–6039, doi:10.5194/acp-12-6009-2012, 2012.

García-Comas, M., Funke, B., Gardini, A., López-Puertas, M., Jurado-Navarro, A., von Clarmann, T., Stiller, G., Kiefer, M., Boone, C. D., Leblanc, T., Marshall, B. T., Schwartz, M. J., and Sheese, P. E.: MIPAS temperature from the stratosphere to the lower thermosphere: Comparison of vM21 with ACE-FTS, MLS, OSIRIS, SABER, SOFIE and lidar measurements, Atmos. Meas. Tech., 7, 3633–3651, doi:10.5194/amt-7-3633-2014, 2014.

Gil-López, S., López-Puertas, M., Kaufmann, M., Funke, B., García-Comas, M., Koukouli, M. E., Glatthor, N., Grabowski, U., Höpfner, Stiller, G. P., and von Clarmann, T.: Retrieval of stratospheric and mesospheric O_3 from high resolution MIPAS spectra at 15 and 10 µm, Adv. Space Res., 36, 943–951, doi:10.1016/j.asr.2005.05.123, 2005.

Glatthor, N., von Clarmann, T., Fischer, H., Funke, B., Gil-López, S., Grabowski, U., Höpfner, M., Kellmann, S., Linden, A., López-Puertas, M., Mengistu Tsidu, G., Milz, M., Steck, T., Stiller, G. P., and Wang, D.-Y.: Retrieval of stratospheric ozone profiles from MIPAS/ENVISAT limb emission spectra: a sensitivity study, Atmos. Chem. Phys., 6, 2767–2781, doi:10.5194/acp-6-2767-2006, 2006.

González-Galindo, F., López-Valverde, M. A., Angelats i Coll, M., and Forget, F.: Extension of a Martian general circulation model to thermospheric altitudes: UV heating and photochemical models, J. Geophys. Res., 110, 09008, doi:10.1029/2004JE002312, 2005.

Gusev, O.: Non-LTE diagnostics of the infrared observations of the planetary atmosphere, PhD thesis, München Universität, Munich, 2002.

Jurado-Navarro, Á. A., López-Puertas, M., Funke, B., García-Comas, M., Gardini, A., Stiller, G. P., and Clarmann, T. V.: Vibrational-vibrational and vibrational-thermal energy transfers of CO_2 with N_2 from MIPAS high-resolution limb spectra, J. Geophys. Res.-Atmos., 120, 8002–8022, doi:10.1002/2015JD023429, 2015.

Kaufmann, M., Gusev, O. A., Grossmann, K. U., Roble, R. G., Hagan, M. E., Hartsough, C., and Kutepov, A. A.: The vertical and horizontal distribution of CO_2 densities in the upper mesosphere and lower thermosphere as measured by CRISTA, J. Geophys. Res.-Atmos., 107, CRI 10-1–CRI 10-19, doi:10.1029/2001JD000704, 2002.

Kaufmann, M., Zhu, Y., Ern, M., and Riese, M.: Global distribution of atomic oxygen in the mesopause region as derived from SCIAMACHY O(1S) green line measurements, Geophys. Res. Lett., 41, 6274–6280, 2014.

Lean, J., Rottman, G., Harder, J., and Kopp, G.: SORCE Contributions to New Understanding of Global Change and Solar Variability, Solar Phys., 230, 27–53, 2005.

Levenberg, K.: A method for the solution of certain non–linear problems in least squares, Quart. Appl. Math., 2, 164–168, 1944.

López-Puertas, M. and Taylor, F. W.: Non-LTE radiative transfer in the Atmosphere, World Scientific Pub., Singapore, 2001.

López-Puertas, M., Zaragoza, G., López-Valverde, M. Á., and Taylor, F. W.: Non local thermodynamic equilibrium (LTE) atmospheric limb emission at 4.6 µm 2. An analysis of the daytime wideband radiances as measured by UARS improved stratospheric and mesospheric sounder, J. Geophys. Res., 103, 8515–8530, 1998.

López-Puertas, M., López-Valverde, M. Á., Garcia, R. R., and Roble, R. G.: A review of CO_2 and CO abundances in the middle atmosphere, in: Atmospheric Science Across the Stratopause, edited by: Siskind, D. E., Eckermann, S. D., and Summers, M. E., Geophysical Monograph Series, 123, 83 pp., American Geophysical Union, 2000.

Lu, H. C., Chen, H. K., Chen, H. F., Cheng, B. M., and Ogilvie, J. F.: Absorption cross section of molecular oxygen in the transition $E^3\Sigma_u^-\, v$= 0–$X^3\Sigma_g^-\, v$ =0 at 38 K, Astron. Astrophys., 520, A19, doi:10.1051/0004-6361/201013998, 2010.

Marquardt, D. W.: An algorithm for least–squares estimation of nonlinear parameters, J. Soc. Indust. Appl. Math., 11, 431–441, 1963.

Mlynczak, M. G., Hunt, L. A., Mast, J. C., Thomas Marshall, B., Russell, J., Smith, A. K., Siskind, D. E., Yee, J.-H., Mertens, C. J., Javier Martin-Torres, F., Earl Thompson, R., Drob, D. P., and Gordley, L. L.: Atomic oxygen in the mesosphere and lower thermosphere derived from SABER: Algorithm theoretical basis

and measurement uncertainty, J. Geophys. Res., 118, 5724–5735, 2013.

Norton, H. and Beer, R.: New apodizing functions for Fourier spectrometry, J. Opt. Soc. Am., 66, 259–264, 1976.

Oelhaf, H.: MIPAS Mission Plan, ESA Technical Note ENVI-SPPA-EOPG-TN-07-0073, 2008.

Offermann, D. and Grossmann, K. U.: Thermospheric density and composition as determined by a mass spectrometer with cryo ion source, J. Geophys. Res., 78, 8296–8304, doi:10.1029/JA078i034p08296, 1973.

Ogawa, S. and Ogawa, M.: Absorption Cross Sections of $O_2(a^1\Delta_g)$ and $O_2(X^3\Sigma_g^-)$ in the Region from 1087 to 1700 Å, Can. J. Phys., 53, 1845–1852, 1975.

Perron, G., Aubertin, G., Desbiens, R., Fehr, T., Niro, F., Kleinert, A., Kiefer, M., Birk, M., and Wagner, G.: MIPAS Level 1b Algorithm Evolutions, in: ESA Living Planet Symposium 2010 (Bergen, Norway), SP-686, ESA Publication Division, 2010.

Picone, J., Hedin, A., Drob, D., and Aikin, A.: NRLMSISE-00 empirical model of the atmosphere: Statistical comparisons and scientific issues, J. Geophys. Res., 107, 1468, doi:10.1029/2002JA009430, 2002.

Raspollini, P., Carli, B., Ceccherini, S., Forzieri, G., Sgheri, L., Ridolfi, M., Carlotti, M., Papandrea, E., Arnone, E., Dinelli, B. M., Castelli, E., Remedios, J., Sembhi, H., Dudhia, A., Lopez-Puertas, M., Funke, B., Flaud, J.-M., von Clarmann, T., Hoepfner, M., Oelhaf, H., Fischer, H., Kiefer, M., Kleinert, A., Chipperfield, M., Perron, G., Aubertin, G., Birk, M., Wagner, G., Gessner, R., Mosner, P., Schmitt, M., Fehr, T., D'Alba, L., and Niro, F.: Level 2 near–real–time analysis of MIPAS measurements on ENVISAT, in: Eight years of MIPAS measurements, SP-686, 011–d2, ESA Publication Division, 2010.

Remsberg, E. E., Marshall, B. T., García-Comas, M., Krueger, D., Lingenfelser, G. S., Martin-Torres, F. J., Mlynczak, M. G., Russell III, J. M., Smith, A. K., Zhao, Y., Brown, C., Gordley, L. L., López-Gonzalez, M. J., López-Puertas, M., She, C.-Y., Taylor, M. J., and Thompson, R. E.: Assessment of the quality of the Version 1.07 temperature-versus-pressure profiles of the middle atmosphere from TIMED/SABER, J. Geophys. Res., 113, 17101, doi:10.1029/2008JD010013, 2008.

Rezac, L., Kutepov III, A., J. R., Feofilov, A., Yue, J., and Goldberg, R.: Simultaneous retrieval of T(p) and CO_2 VMR from two-channel non-LTE limb radiances and application to daytime SABER/TIMED measurements, J. Atmos. Sol.-Terr. Phys., 130–131, 23–42, doi:10.1016/j.jastp.2015.05.004, 2015.

Rienecker, M. M., Suarez, M. J., Gelaro, R., Todling, R., Bacmeister, J., Liu, E., Bosilovich, M. G., Schubert, S. D., Takacs, L., Kim, G.-K., Bloom, S., Chen, J., Collins, D., Conaty, A., da Silva, A., Gu, W., Joiner, J., Koster, R. D., Lucchesi, R., Molod, A., Owens, T., Pawson, S., Pegion, P., Redder, C. R., Reichle, R., Robertson, F. R., Ruddick, A. G., Sienkiewicz, M., and Woollen, J.: MERRA: NASA's Modern-Era Retrospective Analysis for Research and Applications, J. Climate, 24, 3624–3648, doi:10.1175/jcli-d-11-00015.1, 2011.

Sharma, R. D.: Technical Note: On the possibly missing mechanism of 15 µm emission in the mesosphere-lower thermosphere (MLT), Atmos. Chem. Phys., 15, 1661–1667, doi:10.5194/acp-15-1661-2015, 2015.

Smith, A. K., Garcia, R. R., Marsh, D. R., and Richter, J. H.: WACCM simulations of the mean circulation and trace species transport in the winter mesosphere, J. Geophys. Res., 116, D20115, doi:10.1029/2011JD016083, 2011.

Smith, A. K., Harvey, V. L., Mlynczak, M. G., Funke, B., Garcia-Comas, M., Hervig, M., Kaufmann, M., Kyrölä, E., López-Puertas, M., McDade, I., Randall, C. E., Russell III, J. M., Sheese, P. E., Shiotani, M., Skinner, W. R., Suzuki, M., and Walker, K. A.: Satellite observations of ozone in the upper mesosphere, J. Geophys. Res., 118, 5803–5821, doi:10.1002/jgrd.50445, 2013.

Stair, A. T., Sharma, R. D., Nadile, R. M., Baker, D. J., and Grieder, W. F.: Observations of limb radiance with Cryogenic Spectral Infrared Rocket Experiment, J. Geophys. Res.-Space, 90, 9763–9775, doi:10.1029/JA090iA10p09763, 1985.

Stiller, G. P., von Clarmann, T., Funke, B., Glatthor, N., Hase, F., Höpfner, M., and Linden, A.: Sensitivity of trace gas abundances retrievals from infrared limb emission spectra to simplifying approximations in radiative transfer modelling, J. Quant. Spectrosc. Ra., 72, 249–280, doi:10.1016/S0022-4073(01)00123-6, 2002.

Tikhonov, A.: On the solution of incorrectly stated problems and method of regularization, Dokl. Akad. Nauk. USSR, 151, 501–504, 1963.

Trinks, H. and Fricke, K. H.: Carbon dioxide concentrations in the lower thermosphere, J. Geophys. Res.-Space, 83, 3883–3886, doi:10.1029/JA083iA08p03883, 1978.

Trinks, H., Offermann, D., von Zahn, U., and Steinhauer, C.: Neutral composition measurements between 90 and 220 km altitude by rocket-borne mass spectrometer, J. Geophys. Res.-Space, 83, 2169–2176, doi:10.1029/JA083iA05p02169, 1978.

von Clarmann, T.: Smoothing error pitfalls, Atmos. Meas. Tech., 7, 3023–3034, doi:10.5194/amt-7-3023-2014, 2014.

von Clarmann, T. and Echle, G.: Selection of optimized microwindows for atmospheric spectroscopy, Appl. Opt., 37, 7661–7669, 1998.

von Clarmann, T., Glatthor, N., Grabowski, U., Höpfner, M., Kellmann, S., Kiefer, M., Linden, A., Mengistu Tsidu, G., Milz, M., Steck, T., Stiller, G. P., Wang, D. Y., Fischer, H., Funke, B., Gil-López, S., and López-Puertas, M.: Retrieval of temperature and tangent altitude pointing from limb emission spectra recorded from space by the Michelson Interferometer for Passive Atmospheric Sounding (MIPAS), J. Geophys. Res., 108, 4736, doi:10.1029/2003JD003602, 2003.

von Savigny, C. and Lednyts'kyy, O.: On the relationship between atomic oxygen and vertical shifts between OH Meinel bands originating from different vibrational levels, Geophys. Res. Lett., 40, 5821–5825, 2013.

Whitson, M. E. and McNeal, R. J.: Temperature dependence of the quenching of vibrationally excited N_2 by NO and H_2O, J. Chem. Phys., 66, 2696–2700, doi:10.1063/1.434217, 1977.

Zaragoza, G., López-Puertas, M., López-Valverde, M., and Taylor, F. W.: Global distribution of CO_2 in the upper mesosphere as derived from UARS/ISAMS measurements, J. Geophys. Res.-Atmos., 105, 19829–19839, doi:10.1029/2000JD900243, 2000.

Zhu, Y., Kaufmann, M., Ern, M., and Riese, M.: Nighttime atomic oxygen in the mesopause region retrieved from SCIAMACHY O(1S) green line measurements and its response to solar cycle variation, J. Geophys. Res.-Space, 120, 405–9073, 2015.